Copy
RM L51L10a

NACA RM L51L10a

NACA

RESEARCH MEMORANDUM

LONGITUDINAL AERODYNAMIC CHARACTERISTICS OF A MODEL AIRPLANE CONFIGURATION EQUIPPED WITH A SCALED X-1 AIRPLANE WING

By James H. Parks

Langley Aeronautical Laboratory
Langley Field, Va.

NATIONAL ADVISORY COMMITTEE
FOR AERONAUTICS

WASHINGTON
April 11, 1952

NATIONAL ADVISORY COMMITTEE FOR AERONAUTICS

RESEARCH MEMORANDUM

LONGITUDINAL AERODYNAMIC CHARACTERISTICS OF A MODEL AIRPLANE CONFIGURATION EQUIPPED WITH A SCALED X-1 AIRPLANE WING

By James H. Parks

SUMMARY

Results are presented of an investigation at Mach numbers from 0.60 to 1.17 of a rocket-propelled model of an airplane configuration equipped with a scaled X-1 wing of 8-percent-thickness ratio. The data were obtained by analyzing the response of the model to abrupt horizontal-tail deflections. Some effects of adding the wing to the fuselage-tail configuration were determined.

The analysis indicated nonlinearity of the lift-curve slope and static-stability characteristics through the entire Mach number range, though the effects were more pronounced at subsonic speeds. Substantial losses in lifting ability were noted at transonic speeds. Buffeting was indicated at lift coefficients slightly below maximum up to Mach number 0.80. Between Mach numbers of 0.80 and 0.91 severe buffeting occurred at lift coefficients well below the maximum. The configuration exhibited a high minimum drag which was reflected in a low maximum lift-drag ratio. Leading-edge suction is indicated at subsonic speed but gradually approaches zero as the Mach number is increased. Although the stability derivatives varied erratically with Mach number and lift coefficient, a high degree of static stability was exhibited through the entire Mach number range. The damping derivatives varied irregularly with Mach number and lift coefficient but the damping was effective even when the model oscillated through complete stalls. The all-movable tail is shown to be an effective device for changing lift, angle of attack, and pitching moment over the entire speed range and little change in control deflection would be necessary to maintain level-flight conditions from $M = 0.90$ to $M = 1.10$.

INTRODUCTION

The results of one phase of a general research program to determine by means of rocket-propelled vehicles in free flight the effects of various wings on the longitudinal stability, control, drag, and buffeting

characteristics of a general airplane configuration are reported herein. The basic technique is described in detail in reference 1. Briefly, however, the information is obtained by recording and analyzing the model response to intermittent disturbances in pitch induced by deflecting the all-movable horizontal tail in an approximate square-wave program as the speed range is traversed.

The model was launched at the Langley Pilotless Aircraft Research Station, Wallops Island, Va. and had a scaled X-1 wing (unswept 40-percent-chord line, aspect ratio 6, taper ratio 0.5, 8-percent-thick airfoil sections twisted and cambered). Basic aerodynamic data were derived from a flight time history over a Mach number range of 0.6 to 1.17.

SYMBOLS

C_N	normal-force coefficient $\left(\frac{a_n}{g}\frac{W}{qs}\right)$
C_c	chord-force coefficient $\left(\frac{-a_l}{g}\frac{W}{qs}\right)$
C_L	lift coefficient $(C_N \cos \alpha + C_c \sin \alpha)$
C_D	drag coefficient $(-C_c \cos \alpha + C_N \sin \alpha)$
$C_{L_{opt}}$	lift coefficient for maximum L/D
$C_{D_{min}}$	minimum drag coefficient
C_m	pitching-moment coefficient
C_{m_o}	pitching moment at $\alpha = \delta = 0^\circ$
a_n	normal accelerometer reading, feet per second per second
a_l	longitudinal accelerometer reading, feet per second per second
A	aspect ratio $\left(\frac{b^2}{S}\right)$
M	Mach number

[redacted]

R	Reynolds number based on wing mean aerodynamic chord
S	total wing area, square feet
V	velocity, feet per second
W	weight, pounds
b	span of wing, feet
$\bar{c}$	wing mean aerodynamic chord, feet
q	dynamic pressure, pounds per square foot
θ	angle of pitch, radians
I_y	moment of inertia about y-axis, slug-feet^2
α	angle of attack, degrees or radians
δ	deflection of all-movable horizontal tails, degrees
ϵ	downwash angle, degrees
f	frequency of the pitching oscillations, cycles per second
P	period of pitching oscillation, seconds
k	reduced-frequency factor $\left(\frac{2\pi f\bar{c}}{2V}\right)$
t	time, seconds
$T_{1/2}$	time to damp to one-half amplitude, seconds

Subscripts:

$\dot{\alpha} = \frac{d\alpha}{dt}\frac{\bar{c}}{2V}$

$q = \frac{d\theta}{dt}\frac{\bar{c}}{2V}$

The symbols α, $\dot{\alpha}$, δ, and q used as subscripts indicate the derivative of the quantity with respect to the subscript; for example, $C_{L_\alpha} = \frac{dC_L}{d\alpha}$.

[redacted]

MODEL AND APPARATUS

Model

A three-view drawing of the configuration tested is shown as figure 1. Photographs of the model are presented as figure 2. The fuselage-empennage combination was designed as a functional general research vehicle for investigating the effects of various components on stability, control effectiveness, and drag characteristics of airplane configurations. Reasons for the selection of this design are set forth in reference 2.

The longitudinal control surface was an all-movable horizontal tail having the geometric characteristics given in figure 1. The horizontal tail of this model differed from previous models of the program in that wiper plates were installed in the horizontal tail to seal the gap at the vertical-tail juncture. Disturbances in pitch were produced by deflecting the control about a hinge line located at 42 percent of the mean aerodynamic chord by means of a hydraulic control system. The lower vertical tail was used to minimize any effect on the longitudinal oscillations that might arise from coupling of longitudinal and lateral motions.

The wing was constructed of solid aluminum and had an NACA 65-108 ($a = 1.0$) airfoil section with an aspect ratio of 6 and taper ratio of 0.50. The wing had 0° incidence at the root but was twisted to -1° incidence at the tip.

Instrumentation

The model contained a nine-channel telemetering unit which transmitted continuous records of two normal, one longitudinal, and two transverse accelerations, control deflection, angle of attack, total pressure, and a reference static pressure. The total and static pressure locations had been calibrated previously on test models. Atmospheric conditions at altitude were determined from a radiosonde released shortly before the flight.

Launching

The model was boosted to maximum velocity by a 6-inch-diameter solid-fuel Deacon rocket. The combination was launched from a model launching platform (fig. 3) at an angle of approximately 45° from the horizontal. The method of boosting is explained fully in reference 1.

[redacted]

TEST AND ANALYSIS PROCEDURE

Tests

One purpose of the test, in addition to obtaining the basic longitudinal aerodynamic parameters, was to determine a buffet boundary. Because the transonic buffet region covers a small Mach number range and a relatively large lift-coefficient range, a maximum number of control pulses was necessary to insure, insofar as possible, complete coverage of the buffet region without sacrificing stability data. Samples of the resulting traces are shown as figure 4. It may be noted that the control was pulsed through 1 cycle every 1.5 seconds between horizontal-tail deflections of 1.2° (trailing edge down) and -2.0° (trailing edge up).

Mach numbers and dynamic pressures during decelerating flight were calculated from telemetered total and static pressures. The Mach numbers were converted to velocity by means of radiosonde data.

Angles of attack measured by the vane indicator on the nose of the model were converted to angles of attack at the center of gravity of the model by the methods of reference 3.

The Reynolds numbers, based on wing mean aerodynamic chord, attained during the flight are shown as a function of Mach number in figure 5.

Analysis

The methods of analysis with a discussion of assumptions made are described fully in reference 1. Essentially the method consists in analyzing the damped short-period transient oscillations resulting from abrupt horizontal-tail deflections by means of the linearized differential equations of motion for two degrees of freedom. The transverse accelerometer records indicated essentially zero rolling and yawing accelerations throughout the test. The angle-of-attack record is used to determine the period and damping of the oscillations, since these values are least affected by the nonlinearities which are shown to exist in the system.

It should be pointed out that, since the results indicate the existence of nonlinearities, the aerodynamic derivatives obtained should be regarded as average or effective values which exist for the particular test conditions. Some effects of such nonlinear derivatives on the transient motion of an aircraft are treated in detail in reference 4.

Accuracy

A detailed discussion of the accuracy of the basic data is presented in reference 2. The estimated amount of possible systematic errors in C_N and C_c arising from accelerometer calibrations are given in the following table:

M	ΔC_N	ΔC_c
0.80	±0.044	±0.010
1.00	±0.028	±0.007
1.14	±0.022	±0.005

The magnitude of random errors in the data are reflected in the scatter shown by the data points in figure 6. As the time rate of change of the measured quantities decreases with decreasing Mach number, the band of scatter reduces from approximately 0.04 in C_L at the higher Mach number to about 0.02 at the lower Mach numbers.

The Mach number has been estimated to be accurate within 2 percent near $M = 1.00$ with the accuracy somewhat better at higher Mach numbers and somewhat less at lower Mach numbers. The dynamic pressure inaccuracies are believed approximately twice the Mach number errors. The horizontal-tail deflections should be correct within 0.10° and the incremental angle of attack correct within 0.20°.

RESULTS AND DISCUSSION

Lift

Typical lift curves for the complete model are shown in figure 6. The lift curve through a stall obtained with the negative control deflection in the Mach number range from 0.81 to 0.78 shows a hysteresis at the higher angles of attack where C_L for constant α is dependent upon the direction of the angle-of-attack change. This effect has been noted in reference 1 and is believed primarily due to a lag in restoration of attached flow during the recovery from the stall.

The decrease in lift-curve slope in the transonic range evident from these plots is shown more clearly in figure 7 where the lift-curve slopes at two values of lift coefficient are expressed as functions of Mach number. Also shown in this figure are the results of wind-tunnel tests of a similar configuration having a 10-percent-thick wing reported in reference 5. Although differences in configuration and lift coefficient

introduce some discrepancies, the shapes of the curves are quite similar. These results are in agreement with the present concept of mixed flows which predicts a loss of lifting ability in the transonic-speed range for this type wing with the loss extending over a larger Mach number range for the higher lift coefficients.

Some degree of linearity of lift-curve slope over the range of lift coefficients tested is indicated above $M = 1.00$. The nonlinearity shown at the lower Mach numbers is emphasised by the fact that the higher lift coefficients are approaching maximum lift.

The contribution of the horizontal tail to the total lift is expressed as the incremental parameter $\frac{\Delta C_L}{\Delta \delta}$ in figure 7. The nonlinearity of the lift data precludes an accurate determination of this parameter, but the values determined by wind-tunnel tests of the isolated tail plan form, (reference 2) also shown in this figure, indicate that these results are of the correct order of magnitude. In the region near $M = 0.95$ where the largest discrepancies occur, large variations in wing-wake characteristics indicated in references 5 and 6 could be expected to result in large variations in the effectiveness of the tail.

A carpet of lift coefficients attained at constant values of angle of attack through the Mach number range are plotted in figure 8. The increase in Mach number range of the transonic bucket with increase in lift coefficient is evident at angles of attack of 4° and higher, at lower angles of attack the bucket is obscured by the Mach number effects on lift due to camber. These Mach number effects on lift due to camber are shown most clearly on the lift-coefficient curve at zero angle of attack. The rather abrupt decrease in lift coefficient from 0.10 at $M = 0.83$ to 0.02 near $M = 0.90$ is in agreement with the results of reference 7 wherein a loss in camber effectiveness was noted at high subsonic Mach numbers.

Maximum Lift and Buffeting

The model lift reached maximum values up to $M = 0.82$. These data are shown as a maximum lift boundary in figure 9. Some higher lift coefficients were reached at higher Mach numbers but no evidence of stalling was indicated. The test limits above $M = 0.89$ are also shown in figure 9. The differences between the stalled data and the data at at high lift but not stalled are evident in the basic data plots of figure 6.

The values of maximum lift coefficient of 0.88 at $M \sim 0.61$ increasing gradually to 0.96 at $M = 0.82$ are of the correct order of

magnitude. It should be pointed out that these values of maximum lift were obtained under dynamic conditions and, from the results of reference 8, may be somewhat higher than those which would be obtained under static test conditions. The rate of change of angle of attack was of the order of 50° per second which at $M = 0.85$ is a $\frac{\dot{\alpha}\bar{c}}{2V}$ factor of about 0.02°. Above $M \sim 0.85$, the peak lift values reached in this test are below the maximum lift values estimated for this wing at Mach numbers near 1.00.

Also shown in figure 9 are values of lift coefficient above which definite indications of unsteady lift occurred. As reproduced in figure 4, these regions of small-amplitude high-frequency oscillations are well defined. The frequency of these oscillations is essentially constant throughout the time history at 68 to 70 cycles per second which corresponds to the natural frequency of the wing in the first bending mode as determined by vibration tests of the complete model. Thus, from the results of reference 9, these unsteady lift oscillations may be identified as buffet.

At Mach numbers less than approximately 0.80, the buffeting begins at lift coefficients approximately 0.075 lower than maximum lift and appears to be the phenomena commonly referred to as stall buffeting. Between $M = 0.80$ and $M = 0.90$, however, the buffet boundary decreases sharply in lift coefficient while an increase in the maximum lift boundary is indicated. The same effect has been noted previously and reported in reference 10. This buffeting is believed due to the separation resulting from the mixed flows existing on the wing of the model at these Mach numbers. This is substantiated by the fact that the buckets in the lift curves of figure 8 occur at approximately the same Mach numbers as this relatively low lift buffet. The relationship of these two phenomena is discussed more fully in references 9 and 10.

The amplitude response characteristics of the telemetering system precludes a quantitative analysis of these unsteady lift conditions. However, for this particular instrumentation it was determined that the minimum detectable variation in lift coefficient near $M = 0.85$ would be of the order of ± 0.02 which, for practical purposes, can be considered a boundary of incipient buffeting.

For comparative purposes, the boundary at which the full-scale wing buffets with an intensity of $\Delta C_L = \pm 0.02$ as reported in reference 9 is plotted on figure 9. Considering the differences in testing techniques, the agreement is good. Unfortunately, no high-lift data were obtained near $M = 0.95$ from the model to check the rapid increase in buffet boundary shown by the full-scale wing; however, near $M = 1.0$ no buffet was indicated by the model; this result agrees with the full-scale results.

It should be pointed out that, as shown in figure 4, the buffeting persisted to lower lift coefficients (as the angle of attack decreased) than those at which it started while the angle of attack was increasing. This is probably attributable to the combined effects of the aerodynamic phenomena and the structural damping characteristics of the wing. The two effects cannot be separated from these data. Similar effects were noted in reference 11.

Drag

Values of drag coefficient at several constant lift coefficients over the Mach number range are shown in figure 10. Included in this figure are the values of minimum drag coefficient which do not occur at a constant lift coefficient. The effect of lift on the Mach number of the drag rise is apparent, decreasing from $M \approx 0.81$ for $C_L = 0.30$ to $M \approx 0.75$ for $C_L = 0.80$. The increase of drag with lift is also evident. A rapid increase in drag at a constant lift coefficient through the transonic Mach range is shown; for example, C_D increases from 0.037 at $M \approx 0.80$ to 0.124 at $M = 1.0$ for $C_L = 0.3$. These drag values agree favorably with the full-scale results of reference 12, particularly at the higher lift coefficients when the drag due to lift is a predominant factor.

The lift coefficients at which minimum drag occurs are shown in figure 11.

The variation of drag with lift is expressed as $dC_D/dC_L{}^2$ in figure 12. Also shown is the inverse of the lift-curve slope in radians at $C_L \approx 0$. The amount of leading-edge suction (or tilting forward of the resultant aerodynamic force vector) as indicated by the difference between the two curves is seen to decrease with increasing Mach number. At the upper test limit, the resultant vector is approximately normal to the wing. The theoretical limit for maximum leading-edge suction for the wing alone is plotted in the same figure as the parameter $1/\pi A$.

Values of $(L/D)_{max}$ are shown in figure 13 as a function of Mach number. The value decreases from approximately 12.5 near $M = 0.60$ to 4.0 near $M = 0.95$ and remains essentially constant to $M = 1.14$. The decrease shown by this curve at transonic Mach numbers reflects the large increase in minimum drag coefficient which occurs simultaneously with small changes in $dC_D/dC_L{}^2$.

Maximum lift-drag ratios attained by the rocket model of reference 13 which had the same fuselage-empennage combination less the lower

[redacted]

vertical fin and a wing of comparable plan form and airfoil section but sweptback 60° to an aspect ratio of 2.24 are shown also in figure 13. The $(L/D)_{max}$ at the lower Mach numbers is reduced by a factor of about 2 by the changes in configuration but at the supersonic Mach numbers the ratios are relatively unaffected.

The lift coefficient at which these maximum lift-drag ratios occur is shown in figure 14. Although the maximum lift-drag ratio is essentially the same for the two configurations above $M = 1.0$, the optimum lift coefficient is somewhat lower for the sweptback configurations.

Static Stability

The periods of the transient oscillations as measured from the angle-of-attack record are shown in figure 15. These data converted to the static stability parameter C_{m_α} are plotted in figure 16. Considerable variation of static stability with lift coefficient is evident. At the lower Mach numbers the low-lift values vary erratically with a minimum value of -0.037 at $M \approx 0.78$ and a maximum of -0.051 near $M = 0.92$, while in the high-lift-coefficient range the value increases smoothly to -0.055 at $M = 0.85$ and remains essentially constant. With a further increase in Mach number, an increase in C_{m_α} is noted for both lift ranges with the low-lift values increasing the more rapidly. Shown for comparison in figure 16 are the static-stability data for the wingless model of reference 2. In general, the presence of the wing is destabilizing except for a small region in the vicinity of $M = 0.80$ where the wing shows a stabilizing effect on the high-lift data and above $M = 1.05$ where a stabilizing effect is shown on the low-lift data. With the center-of-gravity position used (near 16 percent of $\bar{c}$), the wing itself should add a negative or stabilizing increment to the total stability while downwash and loss of dynamic pressure in the wing wake should add a positive increment. From these data the effects cannot be isolated, but it appears that the losses in stability due to the wake of the wing are predominant. This conclusion is verified in part by the large transonic downwash changes reported for a similar model in reference 5 and for the full-scale airplane in reference 6.

The configuration exhibited a high degree of static stability over the entire Mach number and lift-coefficient ranges as shown by the aerodynamic center locations in figure 17. Increasing lift has a stabilizing effect up to $M = 0.97$ but at higher Mach numbers the effect is reversed. The reasons for these irregular shifts in aerodynamic-center location are not completely known but similar variations have been noted on previous rocket models of reference 1.

It is of interest to note that the periods of the transient longitudinal motion of the model vary quite smoothly with Mach number even though the aerodynamic parameters describing the motion vary erratically.

Damping in Pitch

Values of the time required for the transient oscillations to damp to one-half amplitude are plotted in figure 18. The relatively high values of time required to damp at the high lift coefficients in the region of $M = 0.80$ are due in a large part to the fact that the model oscillated through rather severe stalls. The reduced frequency factor k was 0.0054 near $M = 0.90$. This value may be considered average for the entire test range.

The time increments converted to the damping derivatives $C_{m_q} + C_{m_{\dot{\alpha}}}$ are shown as functions of Mach number in figure 19. Since these data were obtained over large ranges of nonlinear lift coefficients with a minimum number of oscillations, the absolute accuracy of the damping derivatives is open to some question; however, the order of magnitude and the loss of damping ability near $M = 0.90$ agree with previous rocket model tests of references 1, 2, and 13. Damping results determined from full-scale X-1 flight tests are reported in reference 14 wherein similar large decreases in damping-moment coefficient occurred near $M = 0.90$ and some uncertainty was encountered because of the erratic variation of the damping-in-pitch parameter with Mach number.

No damping derivatives were computed for the high lift range between $M = 0.70$ and $M = 0.88$ because the oscillations traversed a range of such severely nonlinear lift coefficients that determinations by the usual methods would yield a rather fictitious result. Some degree of damping exists under these conditions, however, as shown by the actual time required to damp to one-half amplitude in figure 18. The variation is smooth over the Mach number range for the higher lifts but is erratic and abrupt at the low lift coefficients.

The damping derivative for the wing-off models is also shown in figure 19. These values may be considered, for practical purposes, as the C_{m_q} contribution to the total damping. The differences between wing-on and wing-off curves can then be treated as the $C_{m_{\dot{\alpha}}}$ contributed by the presence of the wing. From these assumptions, it appears that the presence of the wing adds a relatively large amount of damping in the system through the lag of downwash except in the region near $M = 0.90$. From the relationship $C_{m_q} + C_{m_{\dot{\alpha}}} \approx C_{m_q}\left(1 + \frac{d\epsilon}{d\alpha}\right)$, it appears that upwash must exist at the tail near $M = 0.92$. This agrees with the results of reference 6 where downwash reversal is shown to occur near $M = 0.92$.

[redacted]

Longitudinal Trim and Control Effectiveness

The trim angles of attack and corresponding lift coefficients at the Mach numbers for which they could be determined are shown in figures 20 and 21. No abrupt trim changes are noted. Increasing lift coefficient amplified the magnitude of the trim changes as shown in figure 21.

The effectiveness of the horizontal control in changing trim lift coefficient and trim angle of attack is shown in figure 22. Although some decrease in effectiveness is evident at the higher Mach numbers, as might be expected from the increased stability, no unusual variations or serious losses are noted.

The effectiveness of the tail in producing pitching moment $\Delta C_m/\Delta\delta$ is plotted in figure 22(c). The variations of effectiveness are small, and the horizontal tail remains an effective device for changing pitching moment throughout the lift and Mach number range.

The value of C_{m_δ} for the wing-off configuration is shown for comparison on the same figure. The presence of the wing has a small effect on the moment-producing ability of the tail with only slight losses indicated near $M = 0.95$.

The values of lift coefficient, angle of attack, and pitching moment at zero control deflection (obtained by linear interpolation) are shown in figure 23. Lift coefficient and angle-of-attack variation with Mach number are what might be expected from previous parts of the discussion and are presented largely for convenience in using the data herein.

The pitching-moment coefficient is for the zero angle-of-attack attitude at zero control deflection and is compared with the wing-off values in figure 23(c). As shown in figure 8 some lift due to camber exists at $\alpha = 0$ except near $M = 0.95$. The location of the wing is such that this lift should contribute a negative pitching moment while the downwash should induce a positive pitching moment. These two effects have apparently cancelled each other near $M = 0.80$ since the presence of the wing does not affect the pitching moment. At lower Mach numbers the effect of downwash seems to be more predominant while, at supersonic speeds, the effect of the wing lift is greater. This result reflects the rearward center-of-pressure shift which is known to exist on wings of this type. Near $M = 0.95$ the presence of the wing adds a relatively large negative increment to the pitching moment even though the wing lift is essentially zero.

The control movement required for level flight with a wing loading of 70 pounds per square foot at 40,000 feet altitude through the transonic

speed range is shown in figure 24. The lift coefficient which would result from a particular control setting as compared to the lift coefficient required for level flight is shown in figure 25. It is evident that flight between M = 0.90 and M = 1.10 could be accomplished at a constant control setting without serious deviations from the level-flight conditions.

CONCLUSIONS

From the flight test of a scale model of an X-1 airplane wing mounted on a basic fuselage-empennage configuration, the following conclusions may be drawn:

1. The lift coefficient varied nonlinearly with angle of attack especially at subsonic speeds. Though substantial losses were indicated at transonic speeds, the configuration exhibited reasonably high values of lift curve slope over the entire Mach number range.

2. The effectiveness of the wing camber in producing lift decreased to nearly zero in the transonic speed range.

3. The configuration buffeted severely at lift coefficients slightly below the maximum up to Mach number 0.80. At Mach numbers from 0.80 to 0.91, the buffet boundary decreased abruptly in lift coefficient. No evidence of buffeting was indicated at Mach numbers of 1.0 or higher.

4. The configuration has a high minimum drag. The leading-edge suction indicated at subsonic speed decreases as the Mach number is increased.

5. The low values of the maximum lift-drag ratios reflect the high minimum drag of the configuration. The values above Mach number 1.00 are slightly less than 4.0.

6. The configuration exhibited a high degree of static stability throughout the Mach number range even though the aerodynamic parameters varied irregularly with lift and Mach number.

7. Light longitudinal damping was indicated near a Mach number of 0.90 but some degree of damping was retained through the entire Mach number range even when the model oscillated through regions of severe stalling. The damping derivatives varied considerably with lift coefficient.

8. No large or abrupt trim changes were noted but an increase in lift coefficient amplified the magnitude of trim change.

[redacted]

9. The all-movable horizontal tail remained an effective device for producing lift, angle of attack, and pitching moment throughout the Mach number range. No large or abrupt changes in effectiveness were indicated.

10. Flight through the transonic speed range could be accomplished with no control difficulties. A fixed control setting could be maintained between $M = 0.90$ and $M = 1.10$ without serious deviation from the level-flight attitude.

Langley Aeronautical Laboratory
National Advisory Committee for Aeronautics
Langley Field, Va.

[redacted]

REFERENCES

1. Gillis, Clarence L., Peck, Robert F., and Vitale, A. James: Preliminary Results from a Free-Flight Investigation at Transonic and Supersonic Speeds of the Longitudinal Stability and Control Characteristics of an Airplane Configuration with a Thin Straight Wing of Aspect Ratio 3. NACA RM L9K25a, 1950.

2. Gillis, Clarence L., and Vitale, A. James: Wing-On and Wing-Off Longitudinal Characteristics of an Airplane Configuration Having a Thin Unswept Tapered Wing of Aspect Ratio 3, as Obtained from Rocket-Propelled Models at Mach Numbers from 0.8 to 1.4. NACA RM L50K16, 1951.

3. Mitchell, Jesse L., and Peck, Robert F.: An NACA Vane-Type Angle-of-Attack Indicator for Use at Subsonic and Supersonic Speeds. NACA RM L9F28a, 1949.

4. Curfman, Howard J., Jr.: Theoretical and Analog Studies of the Effects of Nonlinear Stability Derivatives on the Longitudinal Motions of an Aircraft in Response to Step Control Deflections and to the Influence of Proportional Automatic Control. NACA RM L50L11, 1950.

5. Mattson, Axel T., and Loving, Donald L.: Force, Static Longitudinal Stability, and Control Characteristics of a $\frac{1}{16}$-Scale Model of the Bell XS-1 Transonic Research Airplane at High Mach Numbers. NACA RM L8A12, 1948.

6. Drake, Hubert M., Carden, John R., and Clagett, Harry P.: Analysis of Longitudinal Stability and Trim of the Bell X-1 Airplane at a Lift Coefficient of 0.3 to Mach Numbers Near 1.05. NACA RM L51H01, 1951.

7. Summers, James L., and Treon, Stuart L.: The Effects of Amount and Type of Camber on the Variation with Mach Number of the Aerodynamic Characteristics of a 10-Percent-Thick NACA 64A-Series Airfoil Section. NACA TN 2096, 1950.

8. Gadeberg, Burnett L.: The Effect of Rate of Change of Angle of Attack on the Maximum Lift Coefficient of a Pursuit Airplane. NACA TN 2525, 1951.

9. Purser, Paul E., and Wyss, John A.: Review of Some Recent Data on Buffet Boundaries. NACA RM L51E02a, 1951.

[redacted]

10. Gadeberg, Burnett L., and Ziff, Howard L.: Flight-Determined Buffet Boundaries of Ten Airplanes and Comparisons with Five Buffeting Criteria. NACA RM A50I27, 1951.

11. Gillis, Clarence L.: Buffeting Information Obtained from Rocket-Propelled Airplane Models Having Thin Unswept Wings. NACA RM L50H22a, 1950.

12. Carman, L. Robert, and Carden, John R.: Lift and Drag Coefficients for the Bell X-1 Airplane (8-Percent-Thick Wing) in Power-Off Transonic Flight. NACA RM L51E08, 1951.

13. Vitale, A. James, McFall, John C., Jr., and Morrow, John D.: Longitudinal Stability and Drag Characteristics at Mach Numbers from 0.75 to 1.5 of an Airplane Configuration Having a 60° Swept Wing of Aspect Ratio 2.24 as Obtained from Rocket-Propelled Models. NACA RM L51K06, 1952.

14. Angle, Ellwyn E., and Holleman, Euclid C.: Determination of Longitudinal Stability of the Bell X-1 Airplane from Transient Responses at Mach Numbers up to 1.12 at Lift Coefficients of 0.3 and 0.6. NACA RM L50I06a, 1950.

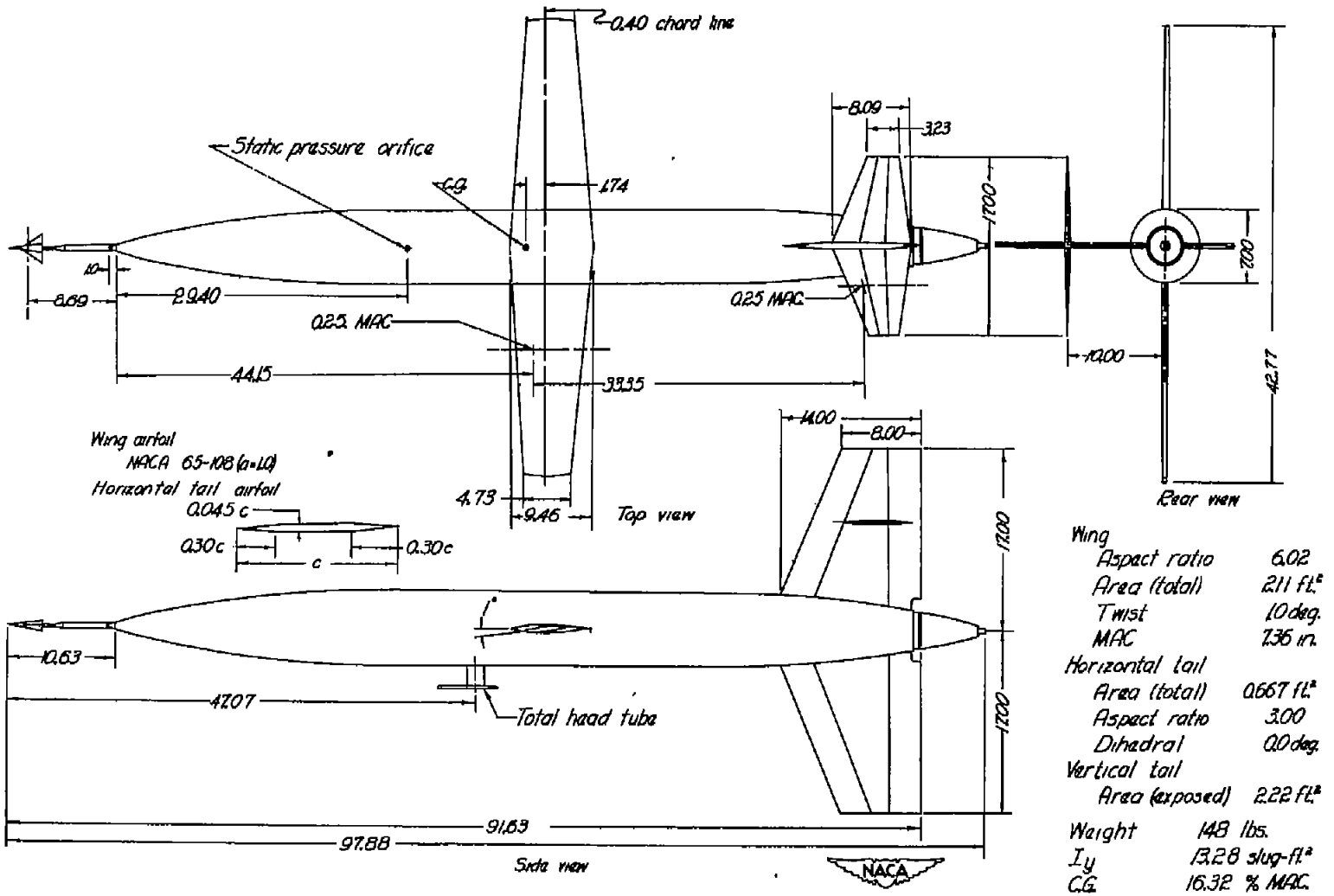

Figure 1.- General arrangement of model. (All dimensions are in inches.)

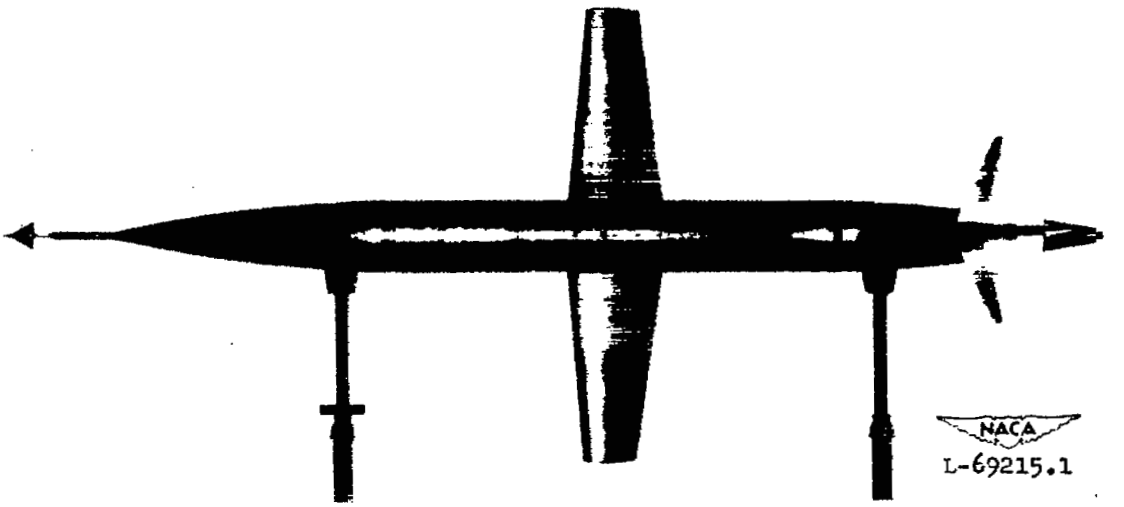

(a) Top view.

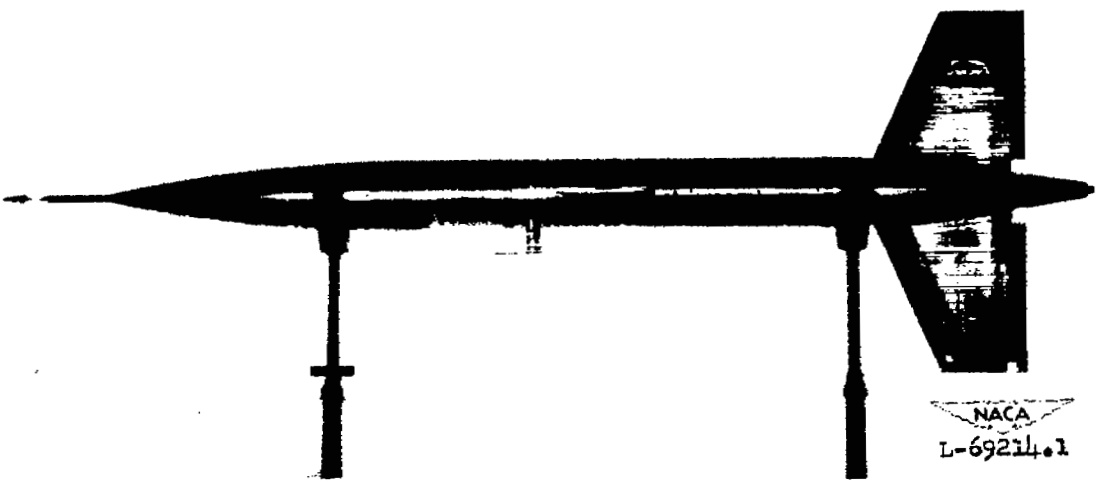

(b) Side view.

Figure 2.- Photographs of the model.

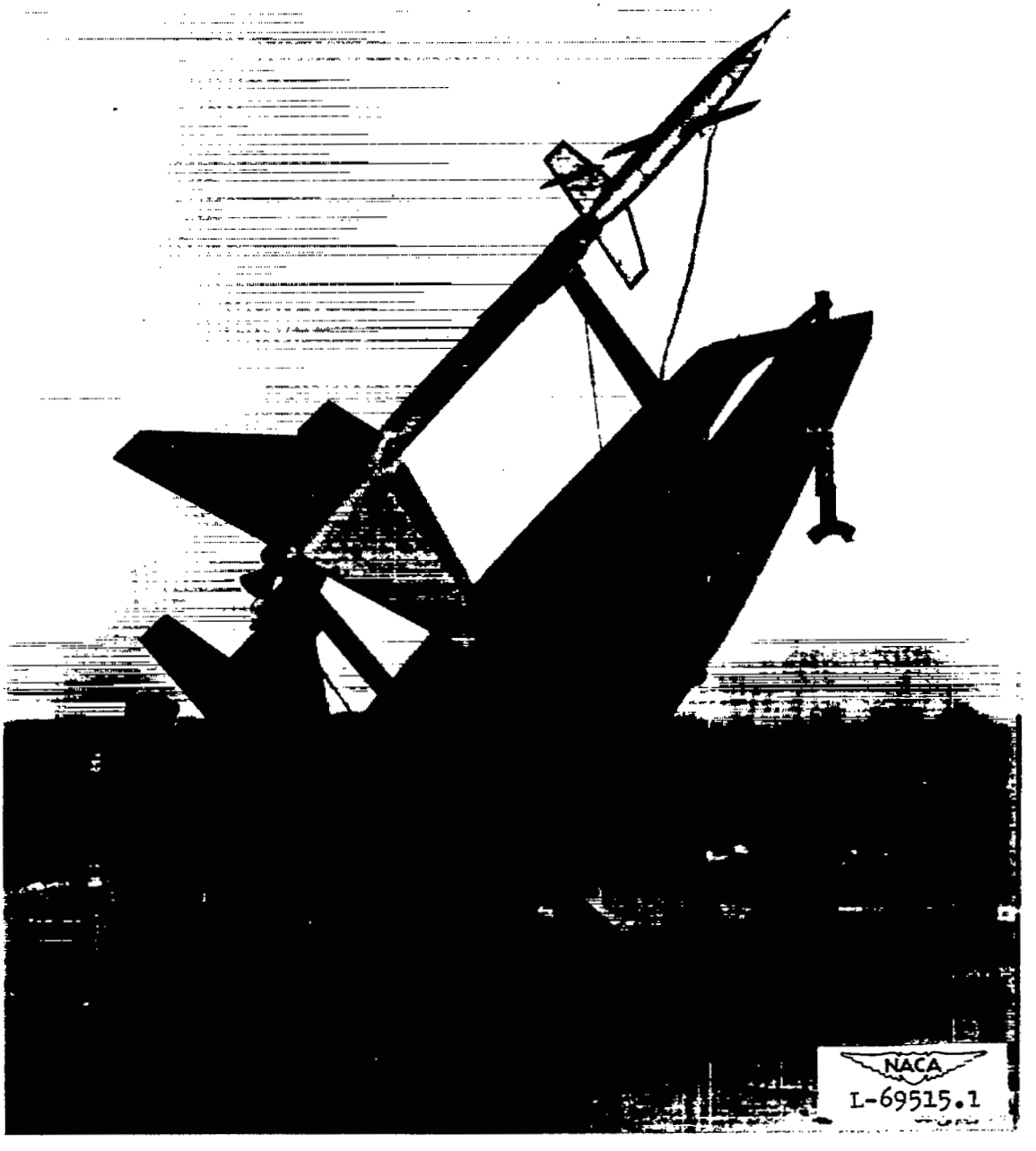

Figure 3.- Photograph of the model-booster combination on the launcher.

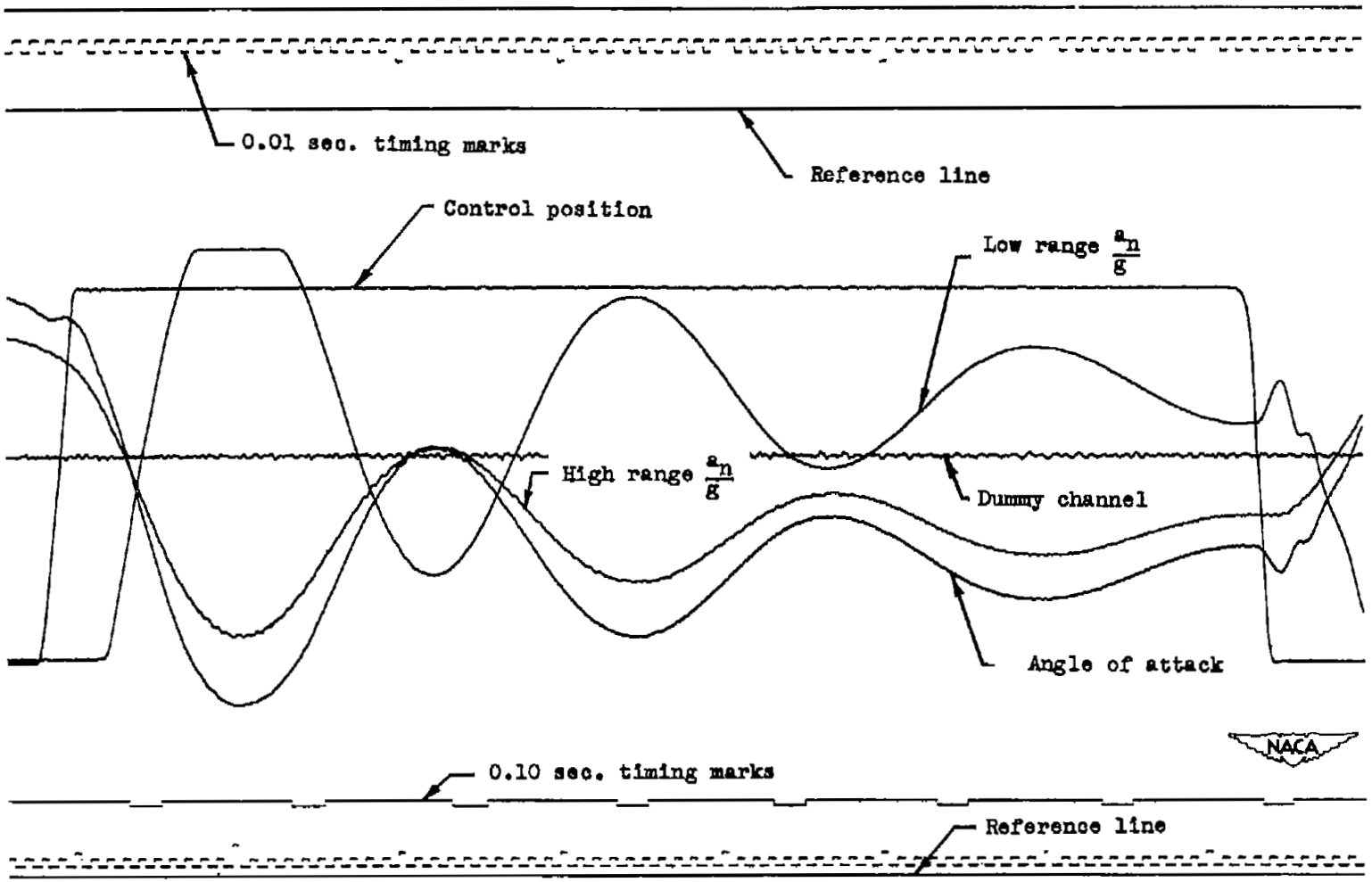

(a) M = 1.12 to 1.03; $\delta = 1.2^{\circ}$.

Figure 4.- Typical portions of the telemeter record at various Mach numbers.

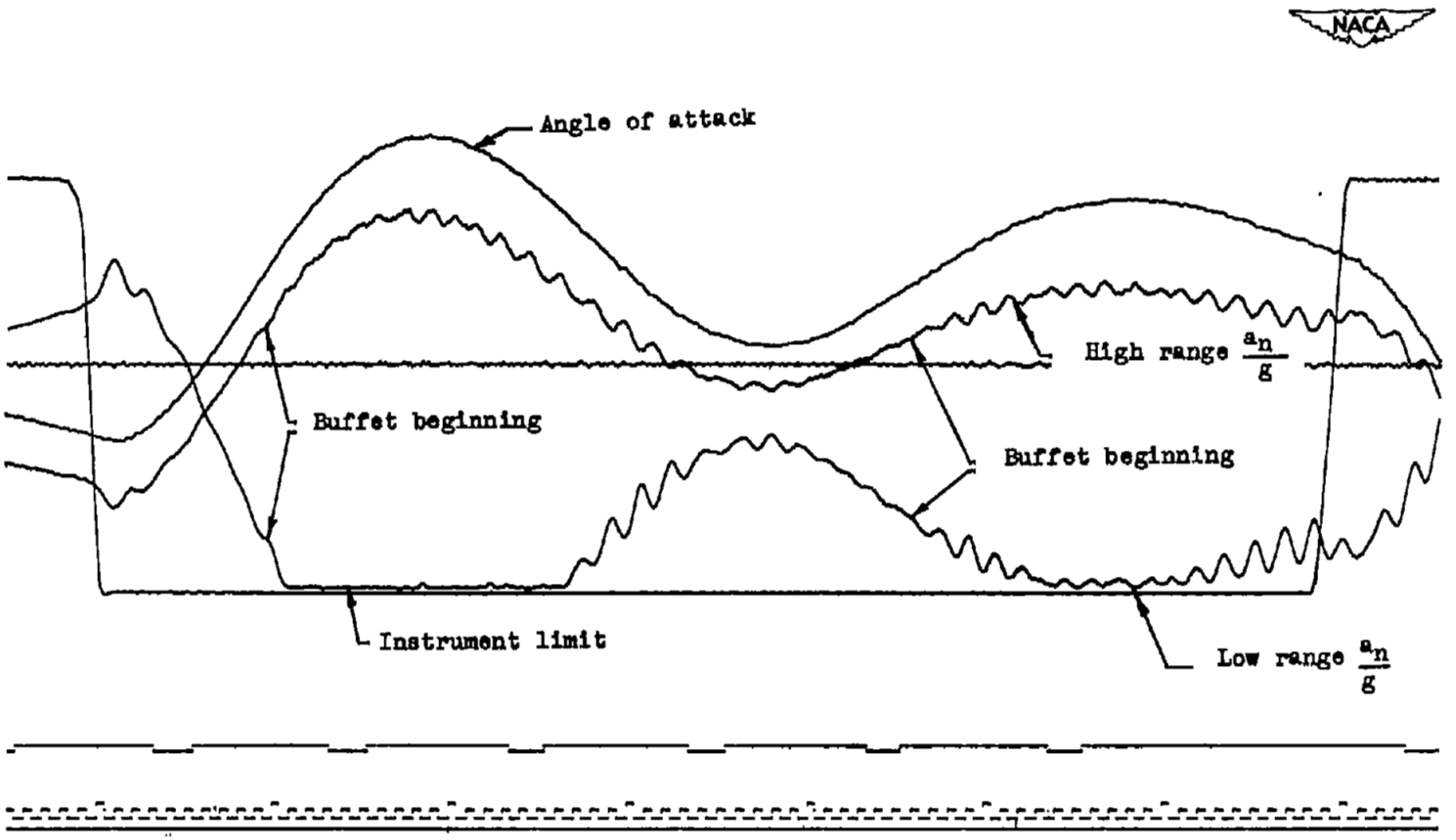

(b) M = 0.91 to 0.86; $\delta = -2.0^\circ$.

Figure 4.- Continued.

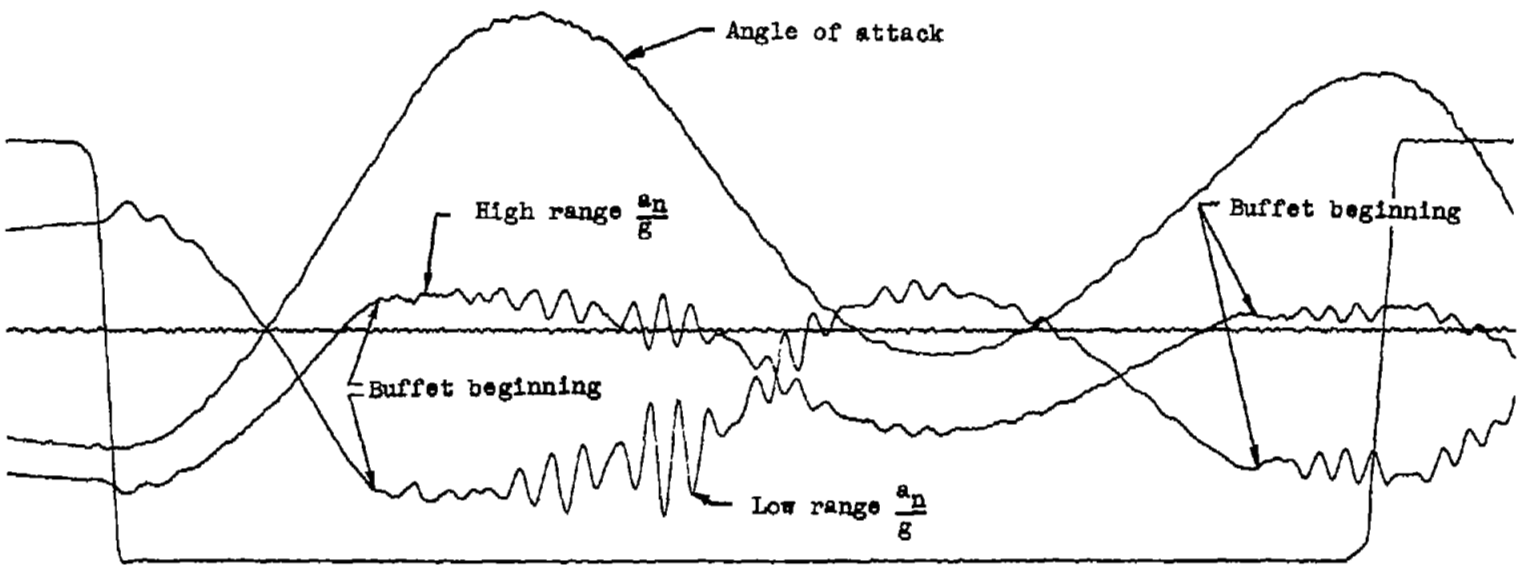

(c) M = 0.76 to 0.73; $\delta = -2.0^{\circ}$.

Figure 4.- Concluded.

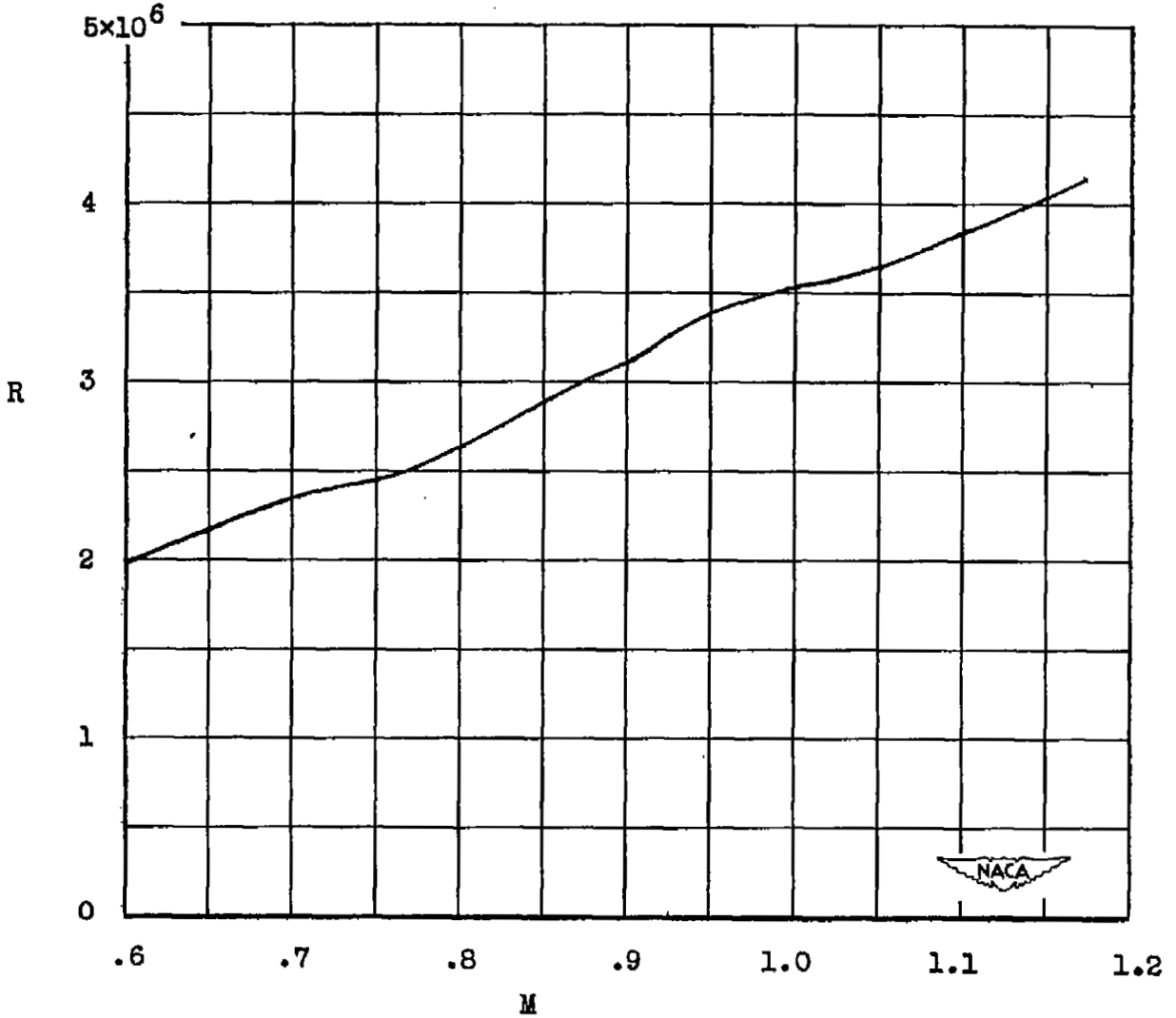

Figure 5.- Reynolds numbers of the test based on the wing mean aerodynamic chord as a function of Mach number.

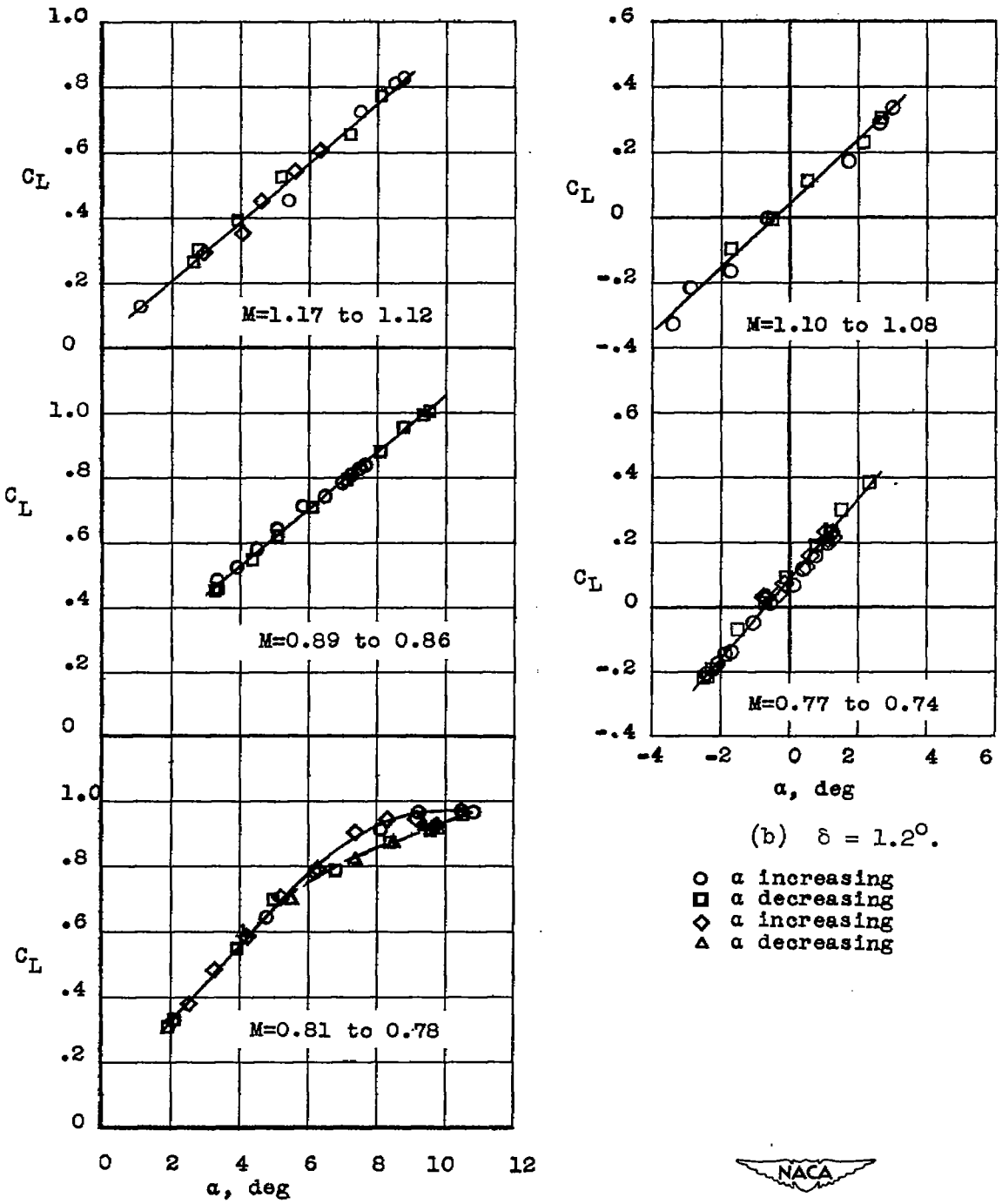

(a) $\delta = -2.0^\circ$.

(b) $\delta = 1.2^\circ$.

Figure 6.- Lift curves at several Mach numbers for the complete model.

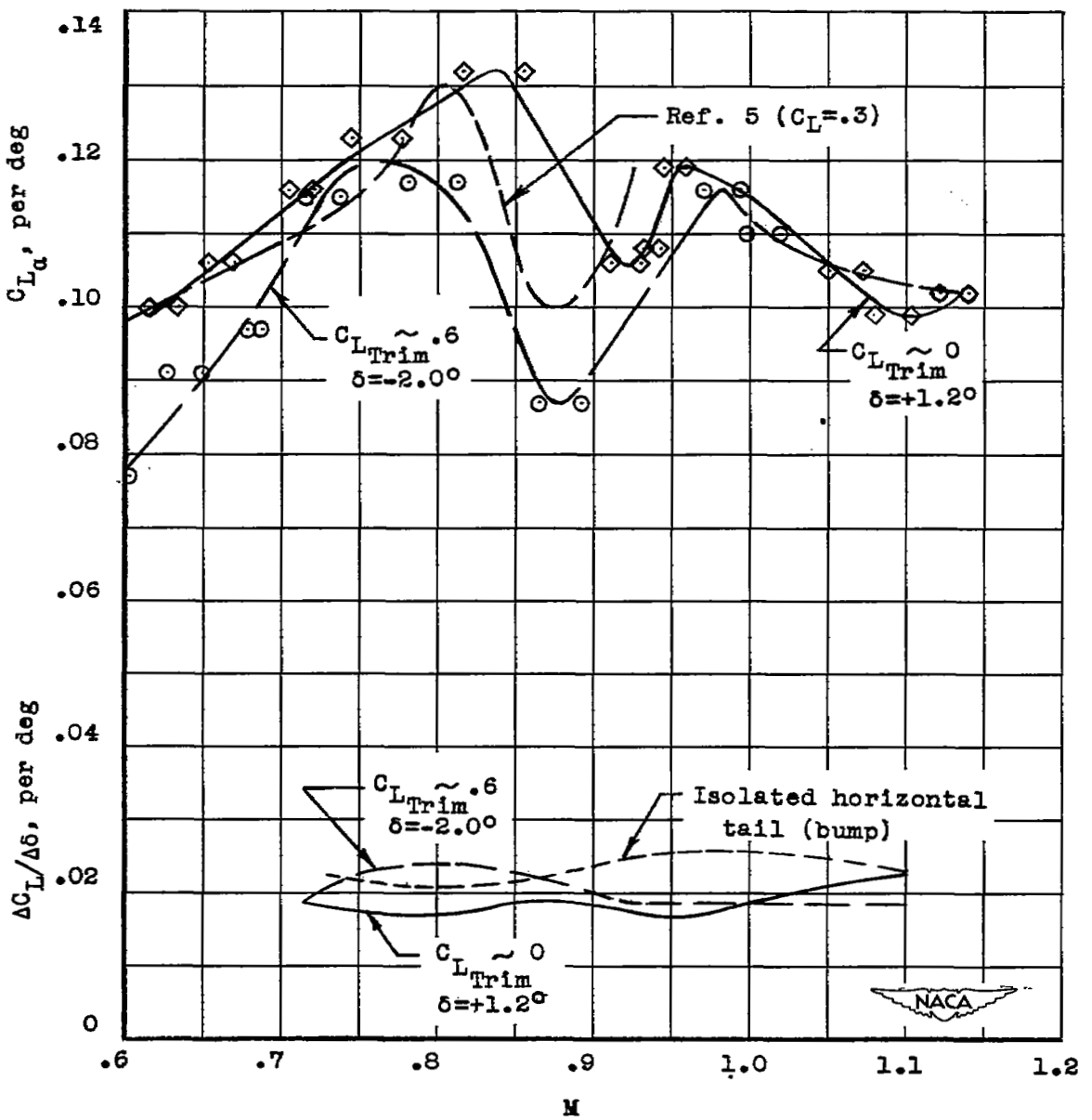

Figure 7.- Lift-curve slopes of the complete model and horizontal tail alone.

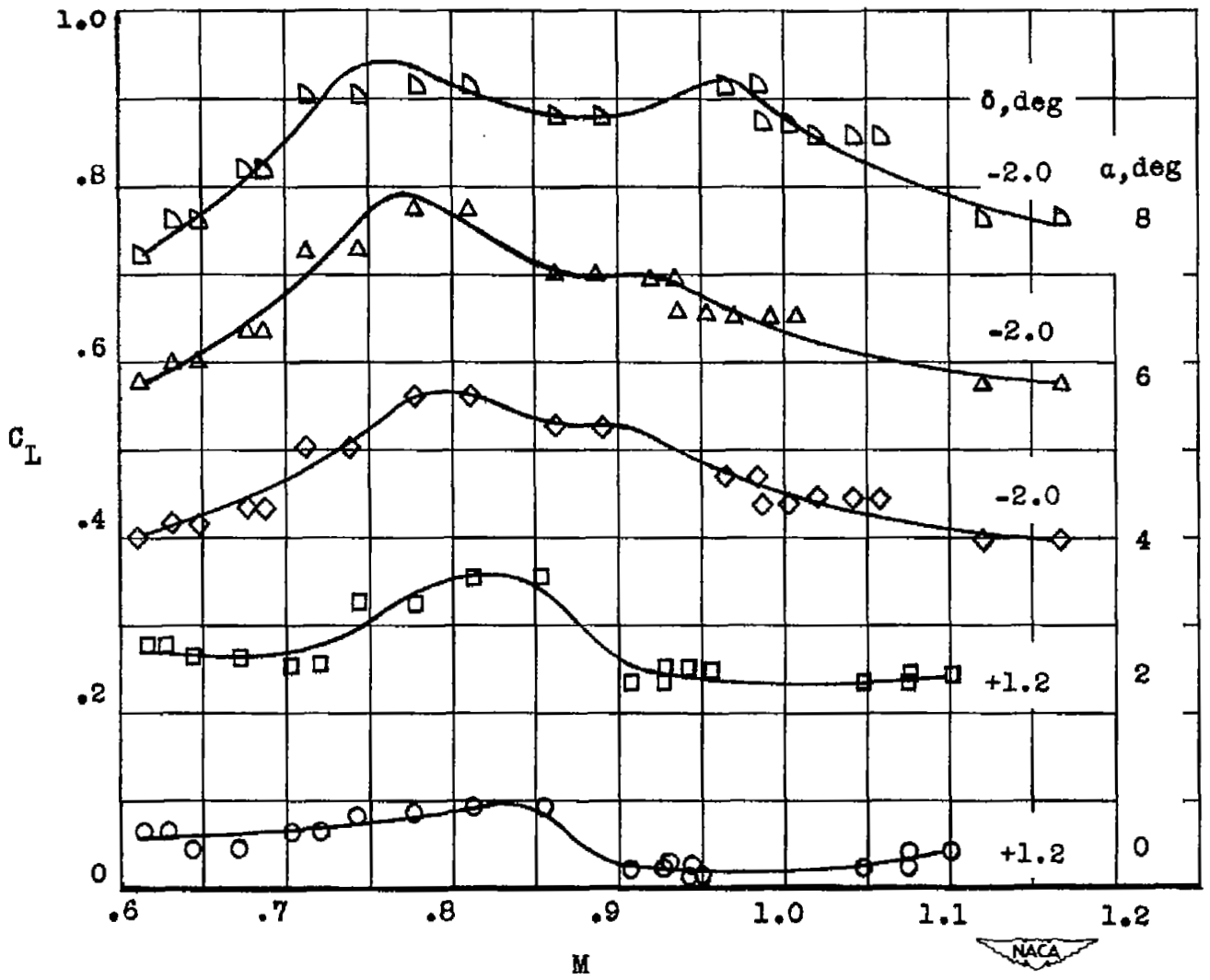

Figure 8.- Variation of lift coefficient with Mach number at several angles of attack.

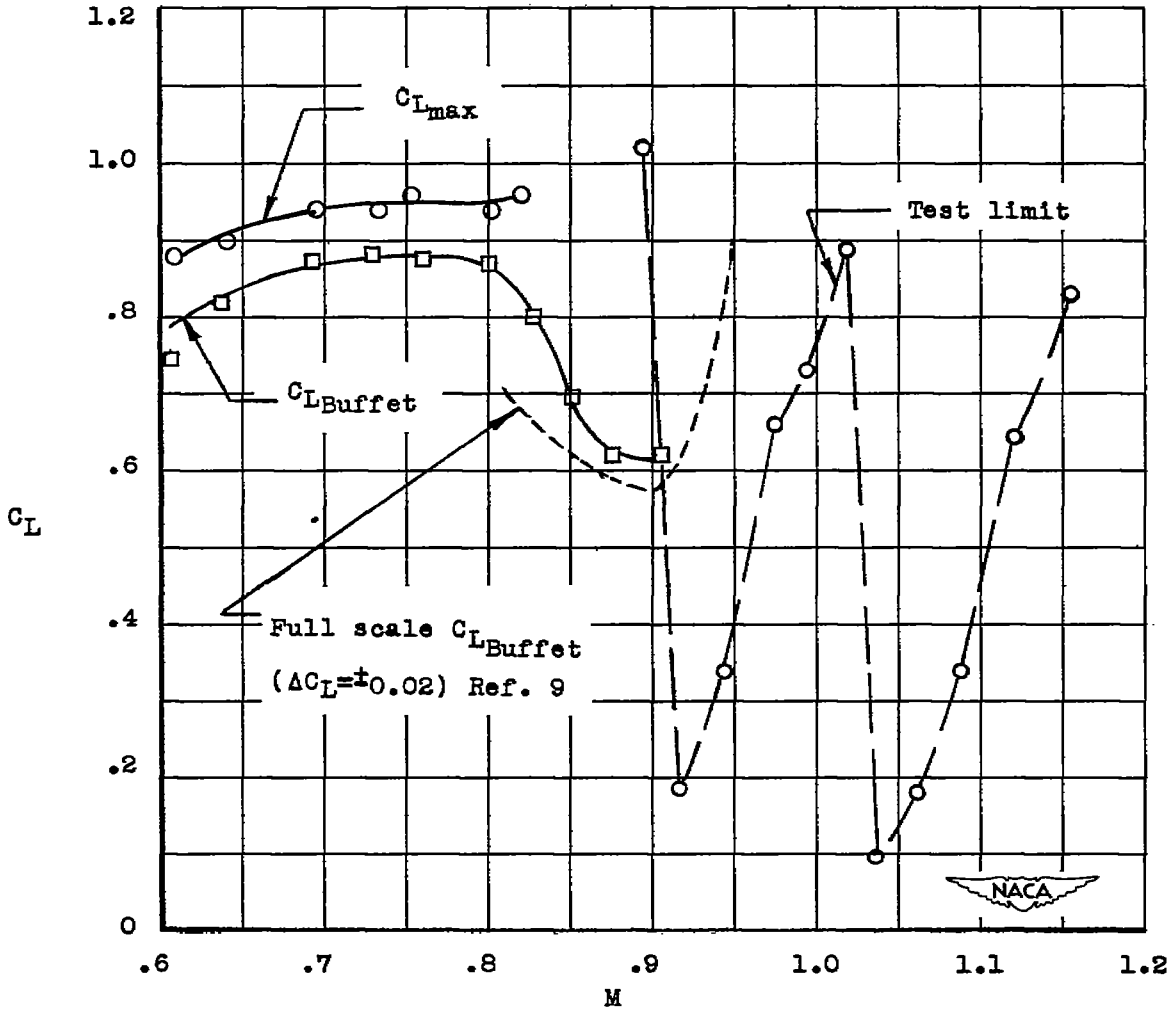

Figure 9.- Boundaries of maximum lift and incipient buffeting.

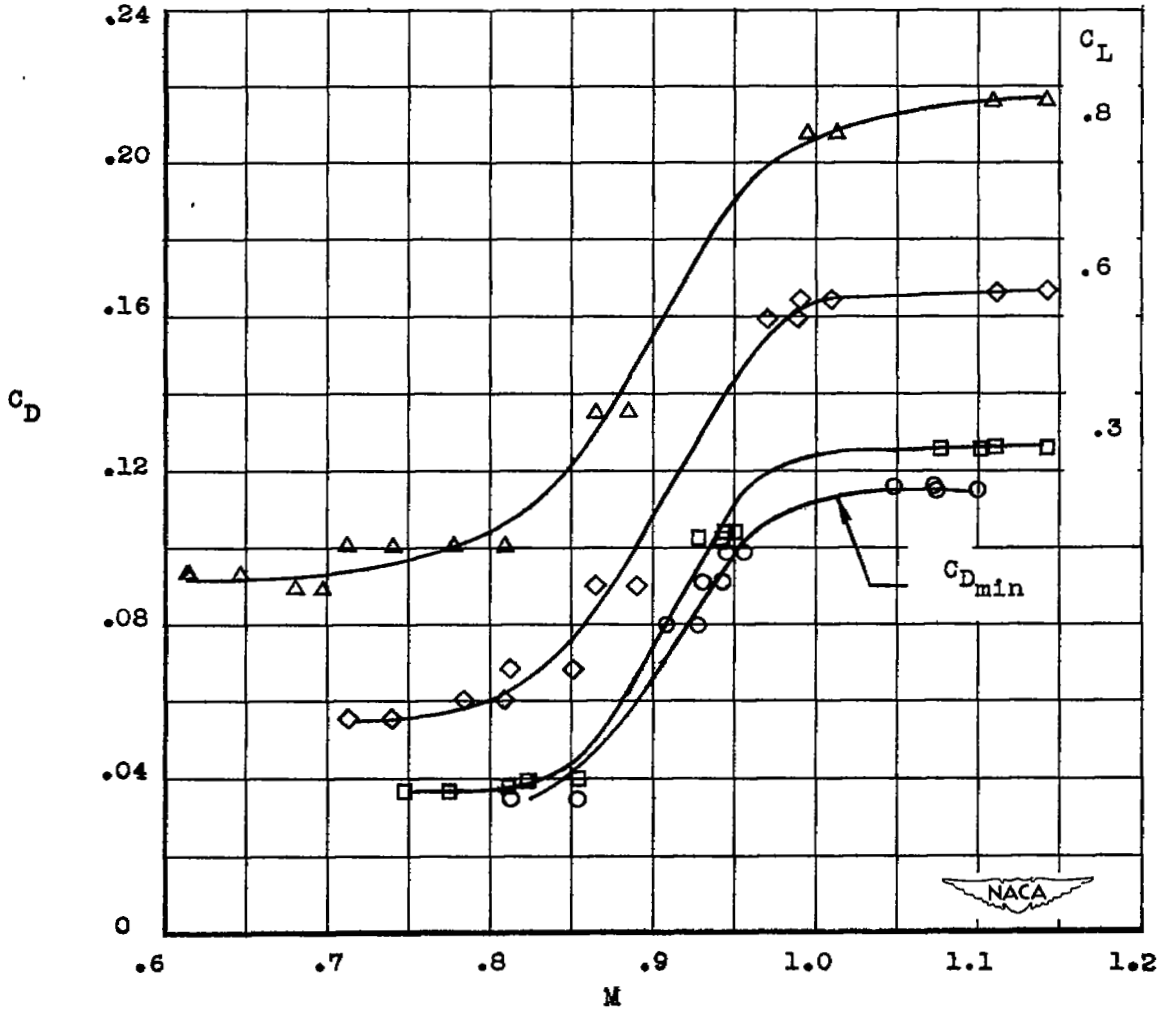

Figure 10.- Drag coefficient at several values of lift coefficient.

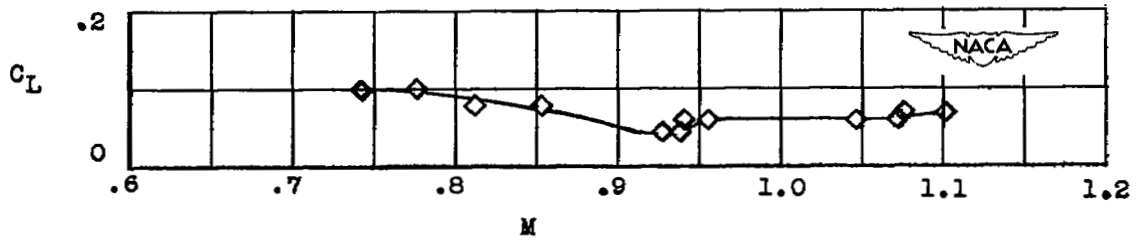

Figure 11.- Lift coefficients at which minimum drag coefficients occur.

[redacted]

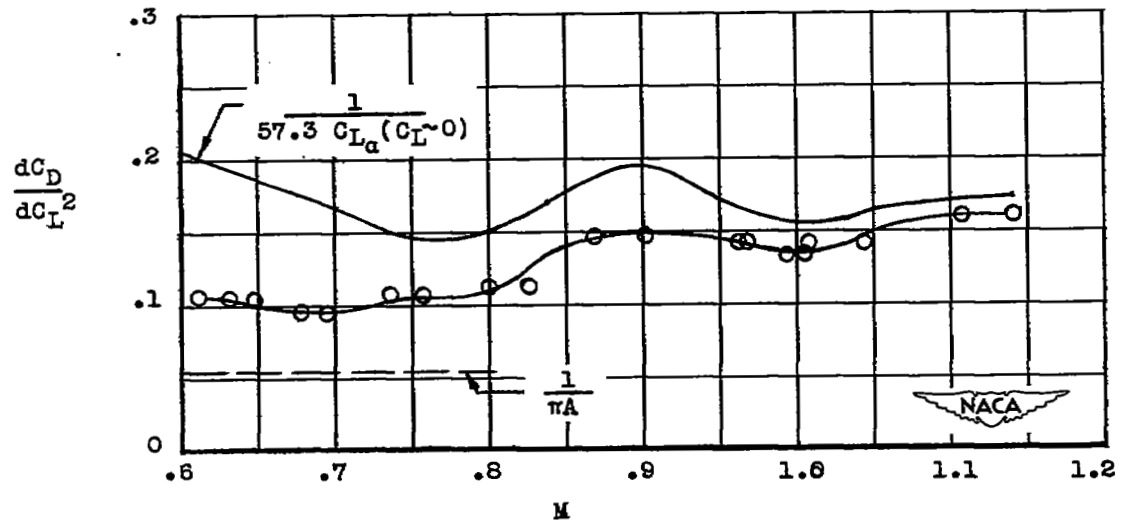

Figure 12.- Effect of lift on drag.

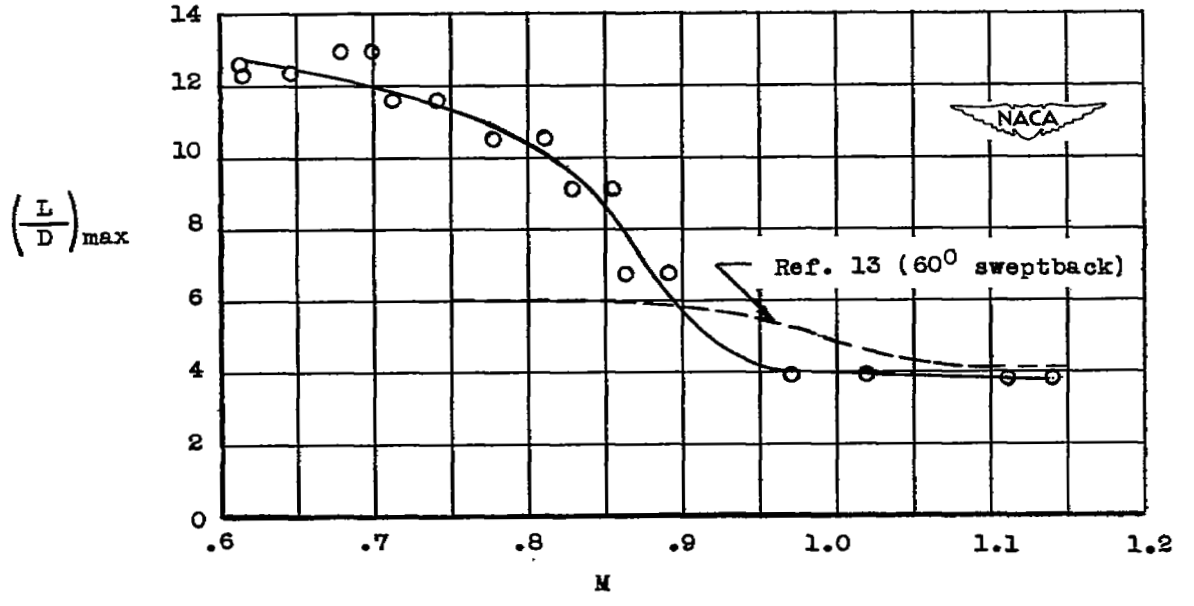

Figure 13.- Maximum lift-drag ratios.

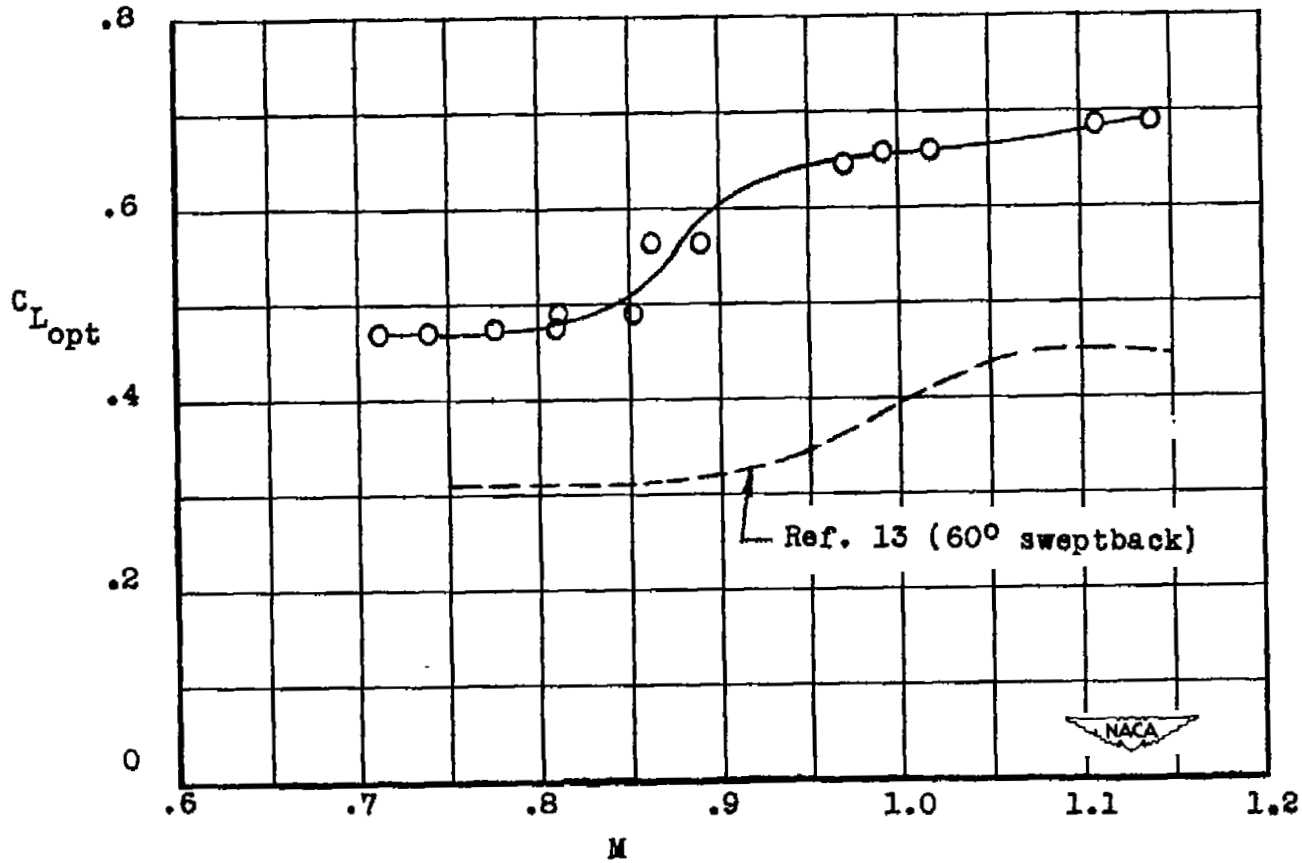

Figure 14.- Lift coefficients at which maximum lift-drag ratios occur.

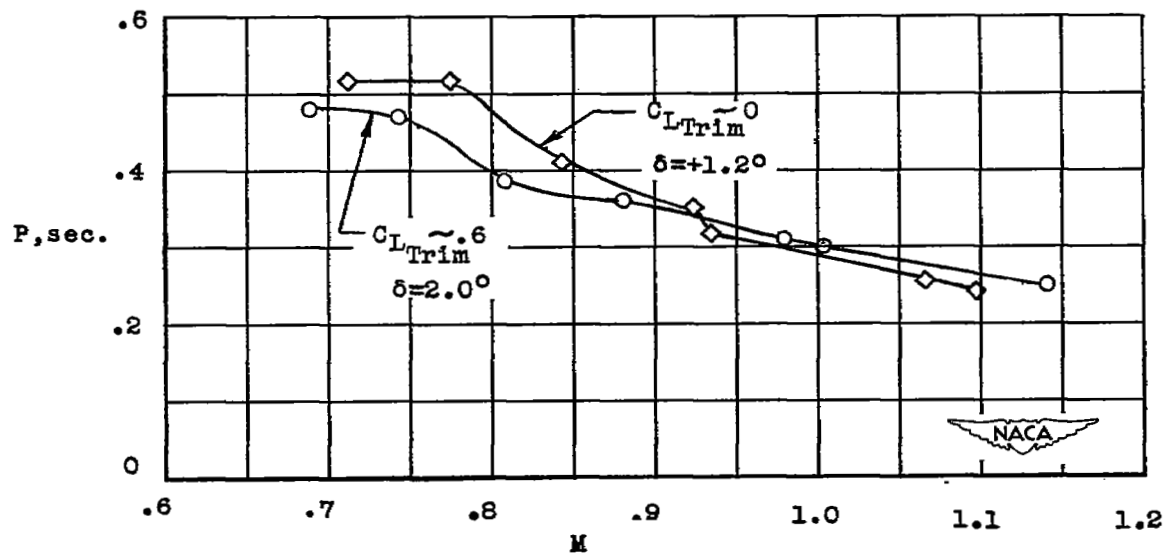

Figure 15.- Periods of the short-period transient oscillations.

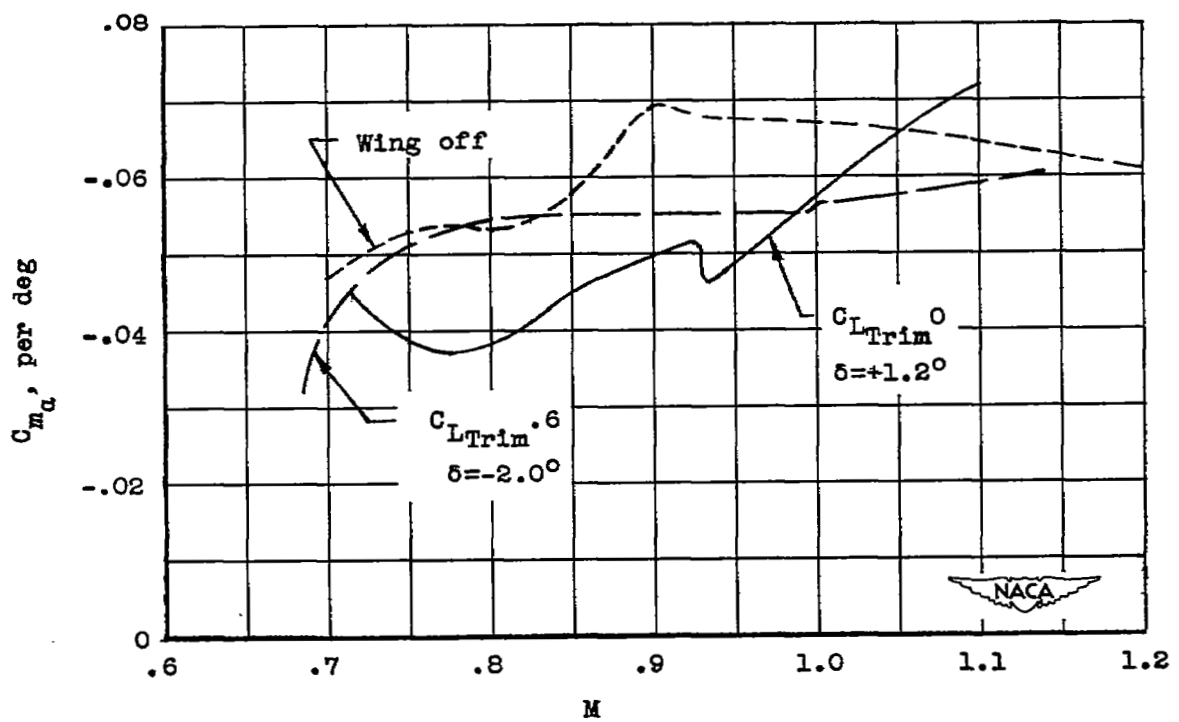

Figure 16.- Variation of the static-stability parameter with Mach number.

[redacted]

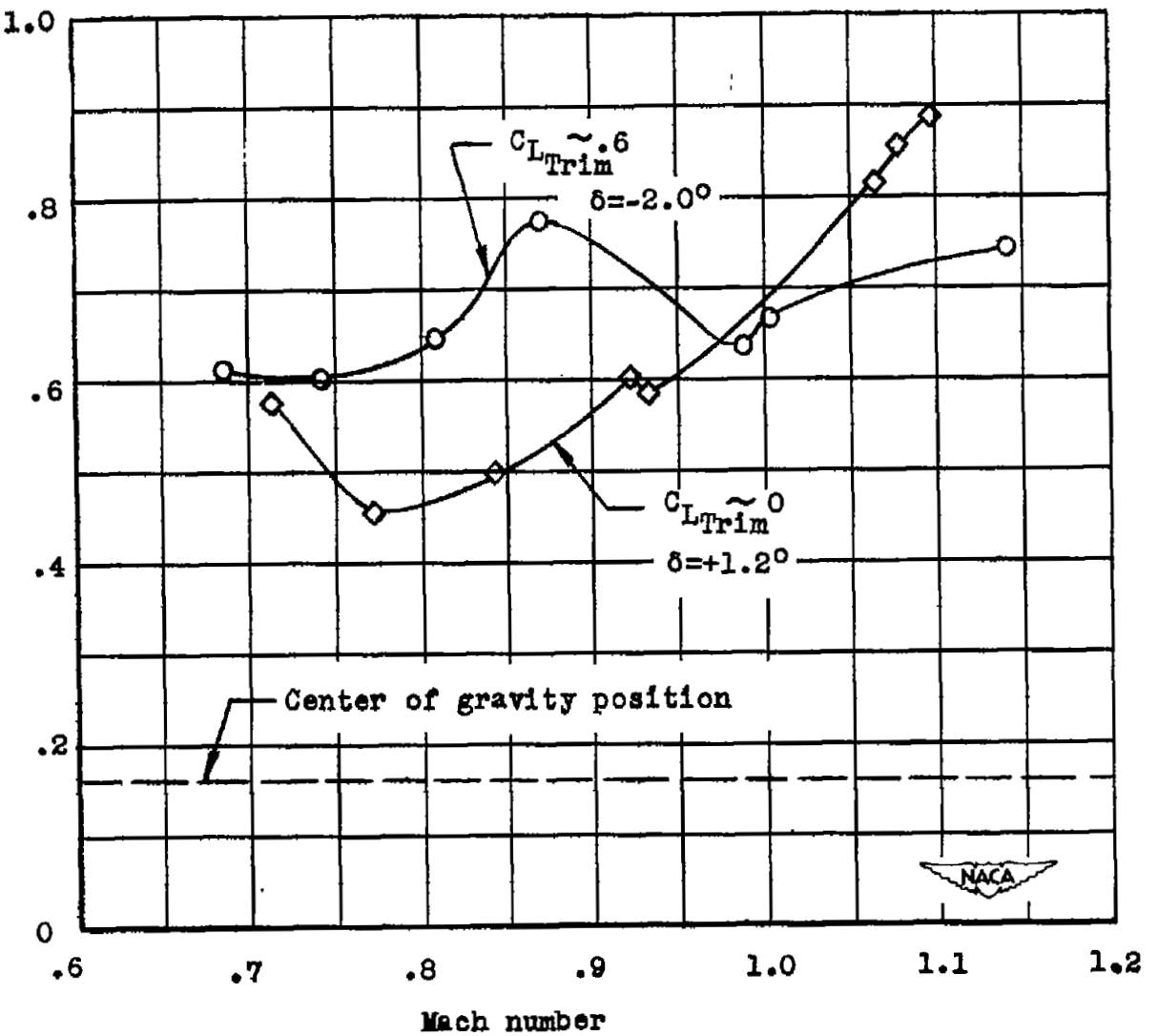

Figure 17.- Variation of the aerodynamic-center location with Mach number.

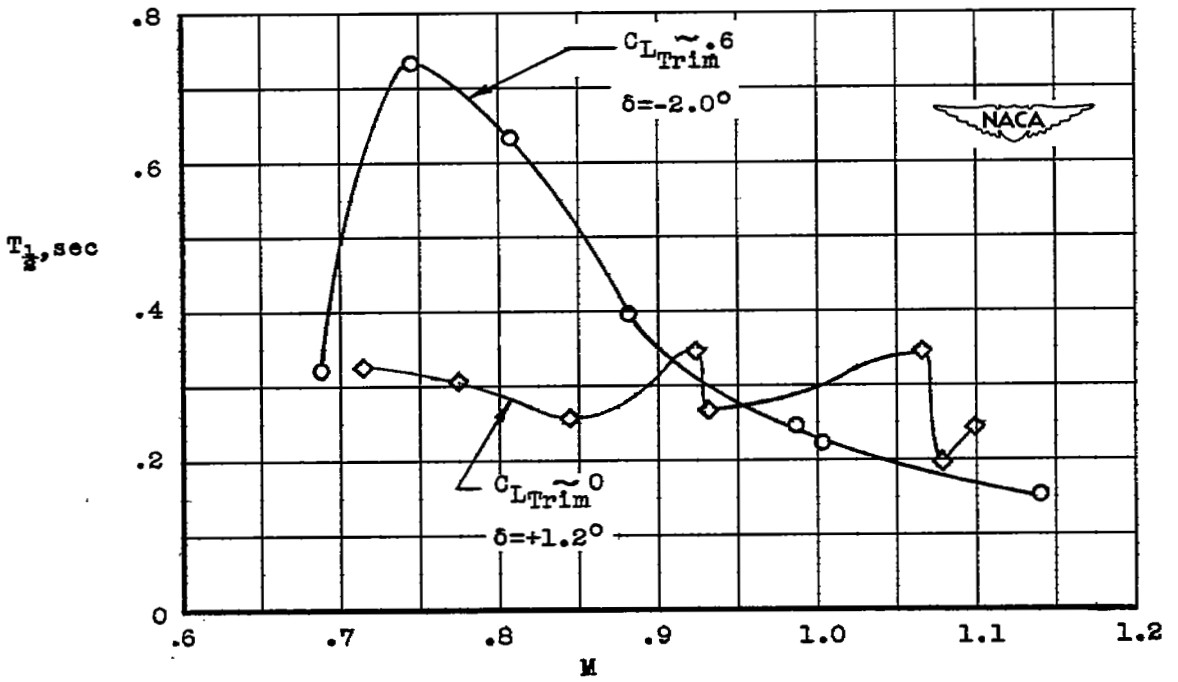

Figure 18.- Time required for the short-period transient oscillations to damp to one-half amplitude.

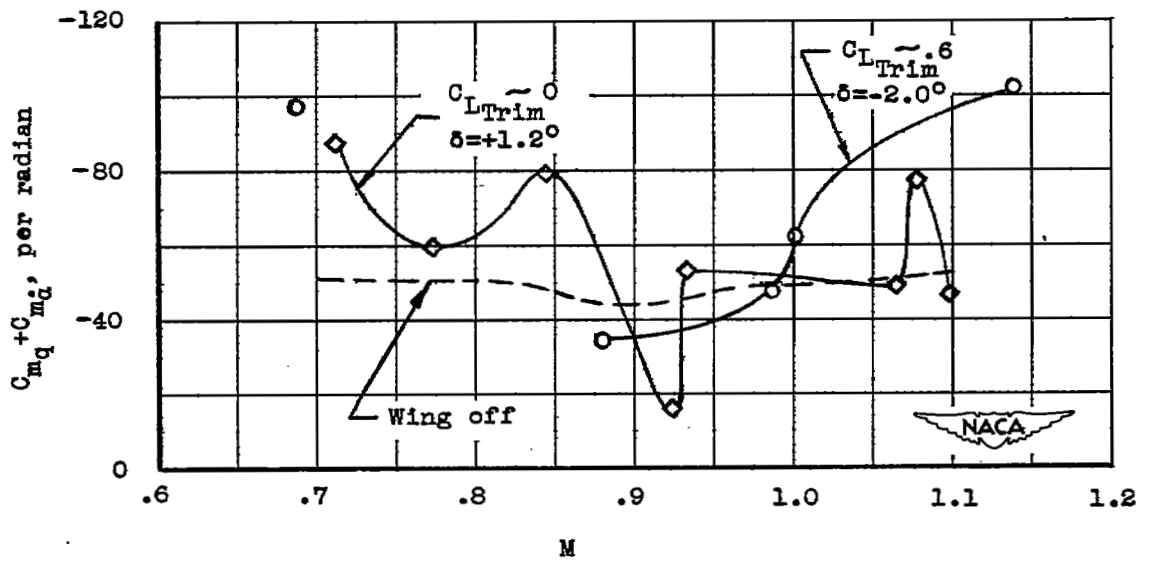

Figure 19.- Variation of the total damping derivative with Mach number.

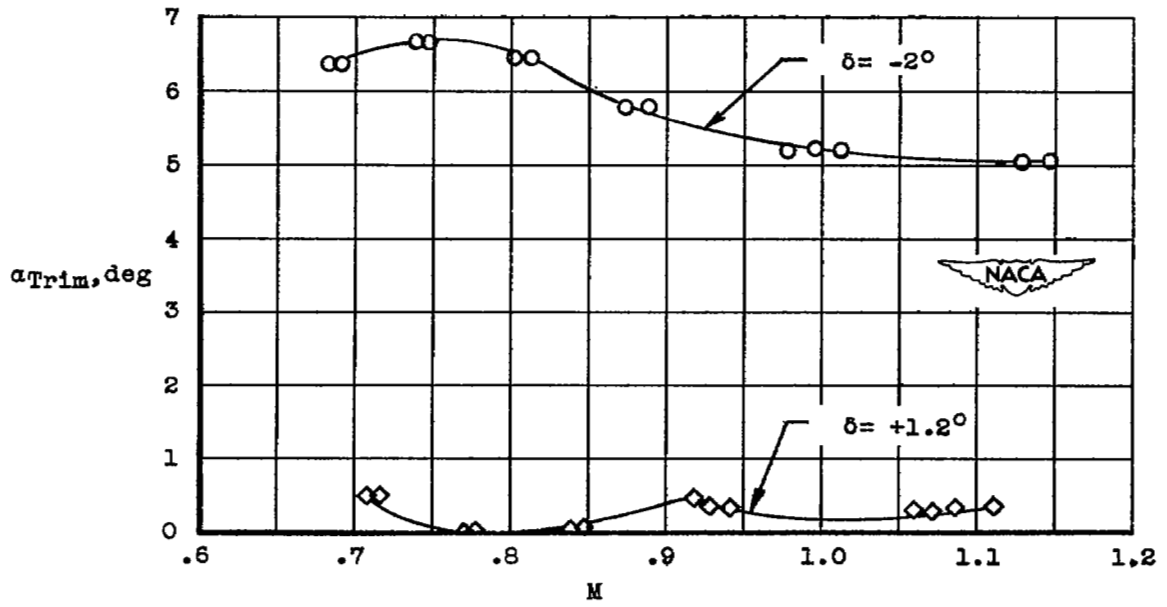

Figure 20.- Variation of trim angle of attack with Mach number.

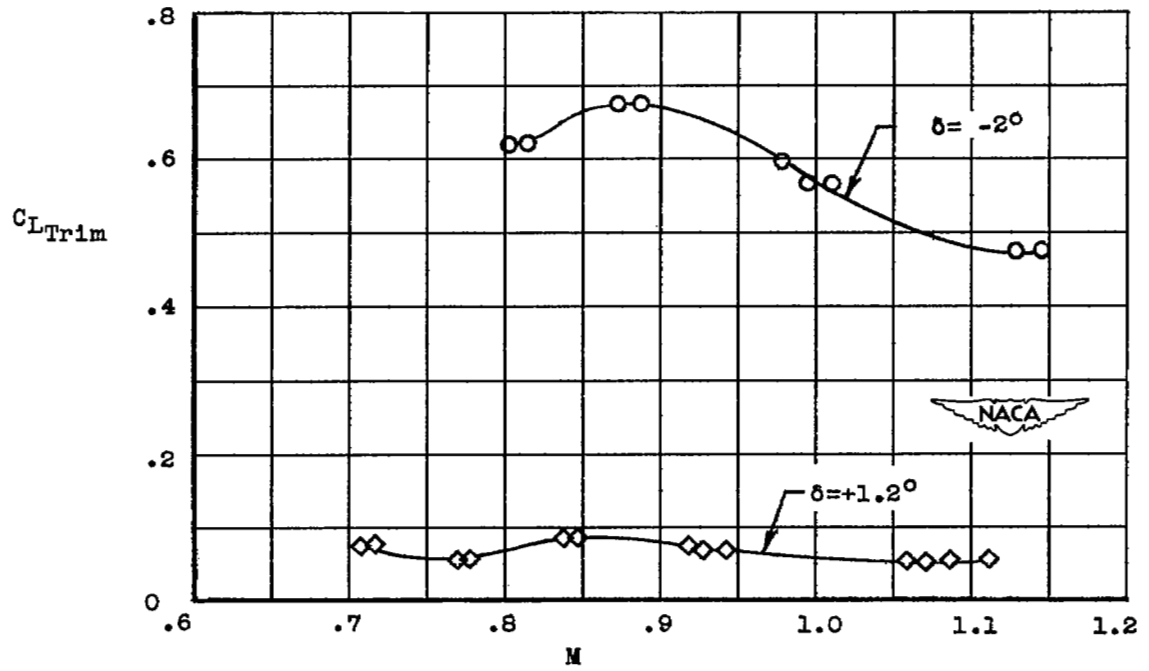

Figure 21.- Variation of trim lift coefficient with Mach number.

[redacted]

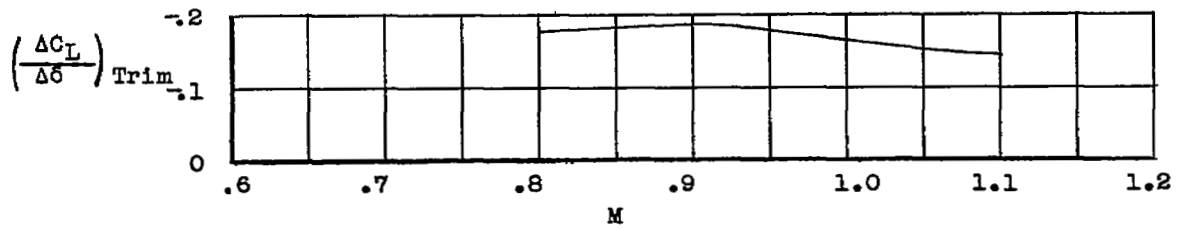

(a) Lift coefficient.

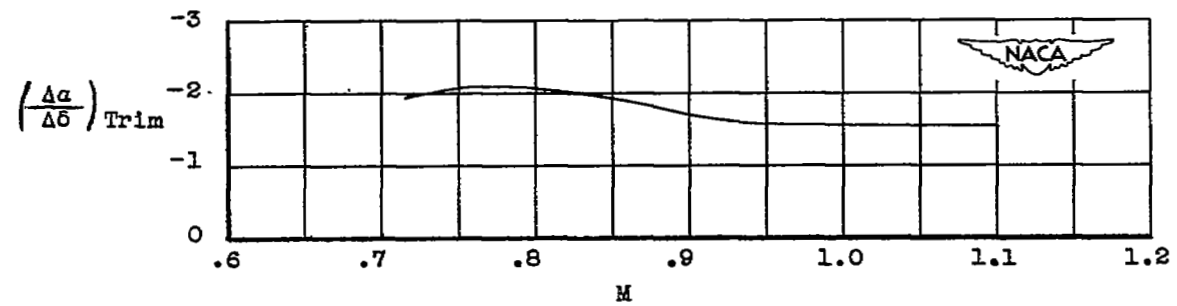

(b) Angle of attack.

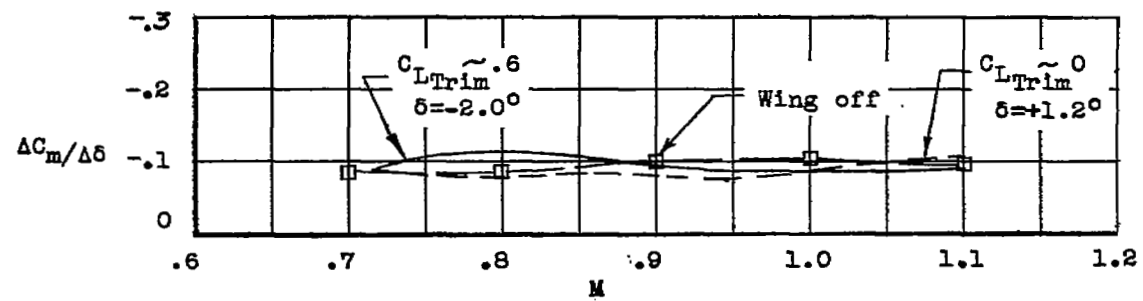

(c) Pitching moment.

Figure 22.- Effectiveness of the all-movable horizontal tail in producing lift, angle of attack, and pitching moment.

[redacted]

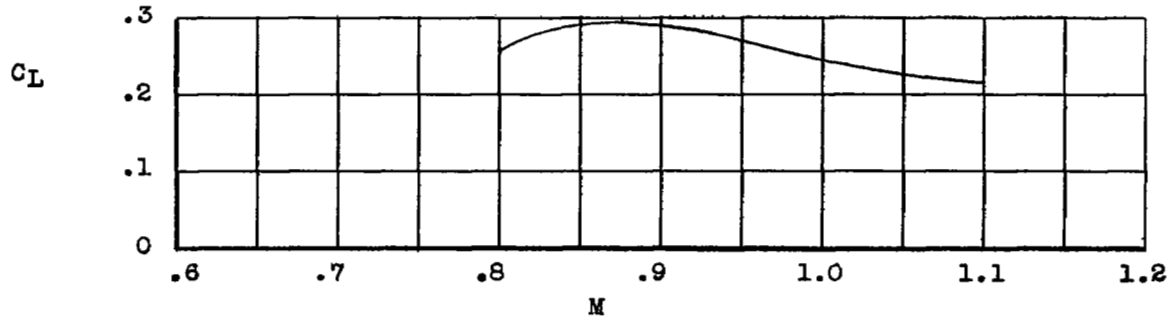

(a) Lift coefficient.

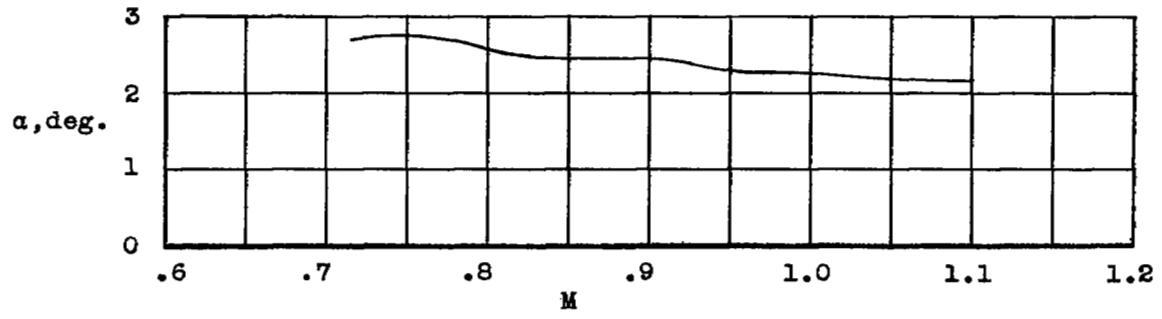

(b) Angle of attack.

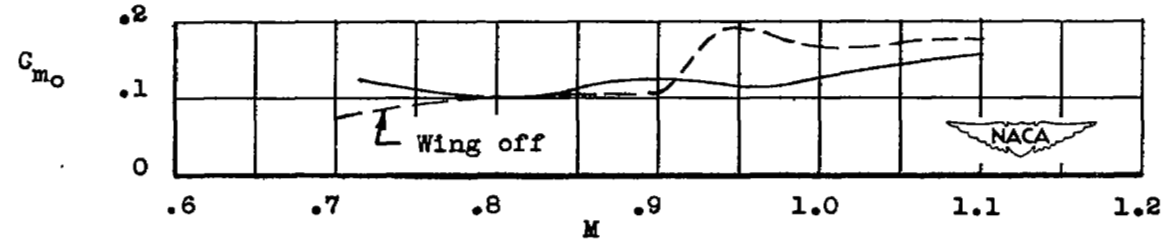

(c) Pitching moment at zero angle of attack.

Figure 23.- Model characteristics with zero control deflection.

[redacted]

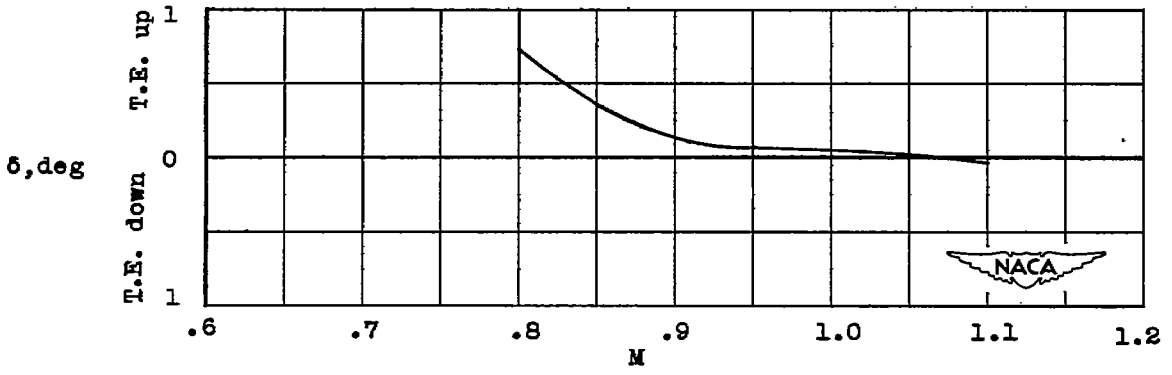

Figure 24.- Control deflection required to maintain level flight at 40,000 feet altitude. $\frac{W}{S}$ = 70 pounds per square foot.

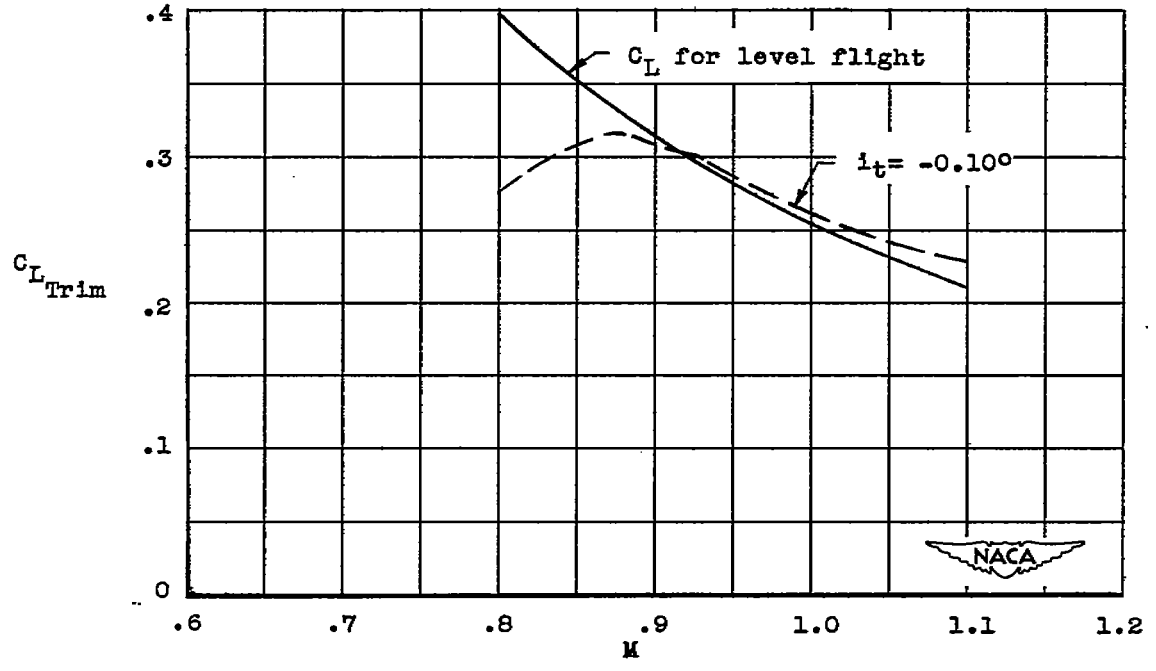

Figure 25.- Effect of constant control deflection of lift coefficient.